WILEY | Hindawi

Research Article

Geochemical Signature of Magmatic-Hydrothermal Fluids Exsolved from the Beauvoir Rare-Metal Granite (Massif Central, France): Insights from LA-ICPMS Analysis of Primary Fluid Inclusions

Matthieu Harlaux, Julien Mercadier, Wilédio Marc-Emile Bonzi, Valentin Kremer, Christian Marignac, and Michel Cuney

Université de Lorraine, CNRS, CREGU, GeoRessources, 54506 Vandœuvre-lès-Nancy, France

Correspondence should be addressed to Matthieu Harlaux; matthieu.harlaux@unige.ch

The Beauvoir granite (Massif Central, France) represents an exceptional case in the European Variscan belt of a peraluminous rare-metal granite crosscutting an early W stockwork. The latter was strongly overprinted by rare-metal magmatic-hydrothermal fluids derived from the Beauvoir granite, resulting in a massive topazification of the quartz-ferberite vein system. This work presents a complete study of primary fluid inclusions hosted in quartz and topaz from the Beauvoir granite and the metasomatized stockwork, in order to characterize the geochemical composition of the magmatic fluids exsolved during the crystallization of this evolved rare-metal peraluminous granite. Microthermometric and Raman spectrometry data show that the earliest fluid (L1) is of high temperature (500 to >600°C), high salinity (17–28 wt.% NaCl eq), and Li-rich ($T_e < -70°C$) with Na/Li ratios ~5. LA-ICPMS analyses of L1-type fluid inclusions reveal that the chemical composition of this magmatic-hydrothermal fluid is dominated by Na, K, Cs, and Rb, with significant concentrations (10^1–10^4 ppm) in rare-metals (W, Nb, Ta, Sn, and Li). This study demonstrates that primary fluid inclusions preserved the pristine signature of the magmatic-hydrothermal fluids in the Beauvoir granite but also in the metasomatized W stockwork, despite the distance from the granitic cupola (>100 m) and interaction with external fluids.

1. Introduction

Rare-metal deposits are mainly associated with peraluminous to peralkaline granites, granitic pegmatites, and carbonatite complexes, which represent major resources for economically strategic metals such as Li, Be, Ta, Nb, Sn, W, and REE [1, 2]. Among these deposits, the LCT (Lithium-Caesium-Tantalum) class of rare-element pegmatites (RMP) and the peraluminous high- and low-phosphorous rare-metal granites (PHP- and PLP-RMG, resp.) constitute the two major groups of rare-metal mineralization [2–5]. In Europe, the Variscan belt represents an important metallogenic province for these two types of rare-metal deposits, which are located mainly in the Bohemian Massif, the Iberian Massif, Cornwall, the Armorican Massif, and the French Massif Central (FMC).

These deposits formed during Carboniferous to Permian times between 330 Ma and 280 Ma in relation to the late-Variscan orogenic evolution [6–10]. In France, the Beauvoir granite represents one of the best examples of a PHP-RMG with a disseminated Sn-Li-Ta-Nb-Be mineralization [5] and was intensively studied during the 1980s–1990s, with the 900 m of continuous core drilling GPF1 from the "Géologie Profonde de la France" program [11]. These studies led to a complete petrological, geochemical, geophysical, structural, and geochronological description of the Beauvoir granite and of its host-environment and to the elaboration of integrated genetic model for this type of rare-metal deposit [12, 13].

The magmatic-hydrothermal evolution of RMG systems is relatively well constrained from a large number of works

based both on natural examples (e.g., [12–15]) and experimental works (e.g., [3, 16–19]). The extreme rare-metal enrichment in these highly peraluminous granitic magmas has generally been interpreted as resulting from crystal fractionation [5]. Deciphering the geochemical composition of the magmatic fluids exsolved from RMG is thus essential to better understand the behaviour of the chemical elements during the late-stage of crystallization and their partitioning between the melt and the fluid phases at the magmatic-hydrothermal transition. Most of these data were obtained from silicate melt inclusion studies, which are considered to represent direct analogues of the composition of the crystallizing magma (e.g., [20–26]). These works reported that late-stage residual melts are enriched in H_2O, fluxing elements (B, F, and P) and incompatible elements (e.g., Be, Sn, Rb, Cs, Nb, Ta, and Li) and reflect the whole-rock bulk composition of the host-granite. At the magmatic-hydrothermal transition, residual fluid yields to phase separation of a low-density vapour phase and a high-density brine [18, 19]. Analysis of the composition of coexisting melt and fluid inclusions trapped during phase separation in low phosphorus RMG showed that most of the trace elements partition into the aqueous fluid phase [21, 25]. However, few data remain available about the trace element composition of fluid inclusions in such magmatic-hydrothermal systems (e.g., [27–29]).

The aims of this work are consequently (i) to determine the trace element composition of the magmatic fluid inclusions trapped in primary quartz and topaz crystals from the Beauvoir granite and to characterize the geochemical signature of these rare-metal-rich magmatic fluids; (ii) to study the partitioning of the minor and trace elements between the coexisting vapour and brine phases resulting from the phase separation during the boiling of the early primary magmatic fluid; (iii) to determine the chemical evolution of the magmatic fluids exsolved from the Beauvoir granite during their interaction with the enclosing micaschists with distance from the granitic cupola.

2. Geological Setting

2.1. Regional Geology of the North French Massif Central.
The Beauvoir granite is located in the Echassières granitic complex in the NE part of the FMC in the Limousin area (Figure 1), which belongs to the internal zone of the European Variscan belt and results from the continental collision between Gondwana and Laurussia during the Upper Paleozoic. The structure of the FMC has been recognized as a stack of metamorphic nappes developed diachronously from Late Silurian to Early Carboniferous, which is constituted by three major tectonic units that are from the north to the south and from top to bottom ([30] and references therein): (i) the Upper Gneiss Unit (UGU), which is composed of migmatitic ortho- and paragneisses and contains the so-called "leptynite-amphibolite complex," formed by the bimodal association of mafic/ultramafic rocks with felsic rocks; (ii) the Lower Gneiss Unit (LGU) which consists of ortho- and paragneisses similar to those of the UGU; and (iii) the Para-Autochthonous Unit (PAU), dominated by metasedimentary units (micaschists, metagreywackes, and quartzites) that experienced low-grade

metamorphism. To the south, these metamorphic units are overthrusted onto the nonmetamorphic rocks of the external zone with its fold-and-thrust belt and its foreland basin.

The Echassières granitic complex intrudes into the Sioule metamorphic series, which is delimited to the west by the Late Carboniferous Sillon Houiller sinistral wrench fault and to the east by the Oligocene Ebreuil and Limagne grabens (Figure 1). The Sioule metamorphic series is located at the northern boundary of the Guéret, St-Gervais, Manzat, and Champ-Valmont granites, which represent large peraluminous cordierite-biotite intrusions emplaced during the Late Devonian to Early Carboniferous at ca. 360–350 Ma [31, 32]. To the south of the Echassières granitic complex, another type of intrusion of biotite porphyritic subalkaline granite (Pouzol-Servant) is emplaced at ca. 330–340 Ma [33]. The Sioule metamorphic series is composed by three lithostructural units, which are from top to bottom [34]: (i) an upper unit of cordierite-bearing migmatite and biotite-sillimanite gneiss, corresponding to the UGU; (ii) an intermediate unit composed by biotite-muscovite paragneiss, corresponding to the LGU; and (iii) a lower unit formed by biotite-muscovite micaschists, which is correlated with the PAU. This series experienced two major synmetamorphic events [35, 36]: (i) a HP D_0 event coeval with eclogitic-granulitic metamorphism at ca. 430–400 Ma; and (ii) a MP-MT D_2 event coeval with the top-to-the-NW shearing at ca. 365–350 Ma.

2.2. Structure and Age of the Echassières Granitic Complex.
The Echassières granitic complex includes an early W-bearing quartz-vein system, the so-called La Bosse stockwork, and at least three successive granitic units that intruded into the micaschists of the PAU [12, 13]. From oldest to youngest, these granitic units are (Figure 2): (i) the La Bosse granite, which is concealed at depth and is presumed to be related to the formation of the W deposit; (ii) the Colettes granite, which is a porphyritic biotite-muscovite-cordierite granite that overprints the La Bosse stockwork; and (iii) the Beauvoir granite, which consists of a topaz-lepidolite-albite granite with disseminated Sn-Li-Ta-Nb-Be mineralization that crosscuts the Colettes granite. The GPF1 drill hole intersected the roof and bottom of the Beauvoir granite at depths of −100 m and −880 m, respectively, below the current surface [11]. This drill hole allowed the identification of a vertical internal zoning in the Beauvoir granite (Figure 2) with three main granitic units emplaced successively, which are separated by magmatic layering and show a magmatic foliation underlined by lepidolite. From the lowest to the upper, these units are [12, 13] (i) B3 facies (−880 to −750 m), which contains euhedral pink-colored K-feldspars, zinnwaldites, and hosts commonly micaschists enclaves with quartz-ferberite veins; (ii) B2 facies (−750 to −450 m) consisting of a lepidolite-rich granular granite with idiomorphic quartz crystals and small amounts of K-feldspars; (iii) B1 facies (−450 to −100 m) corresponding to an albite-lepidolite-rich granite containing globular quartz crystals with typical "snowball" textures and rare anhedral perthitic K-feldspars. Generally, the abundance of accessory minerals (topaz, cassiterite, columbite-tantalite, microlite, and Li-Be phosphates) tends to increase upward from the B3 to the B1 facies, the latter being the most evolved. This
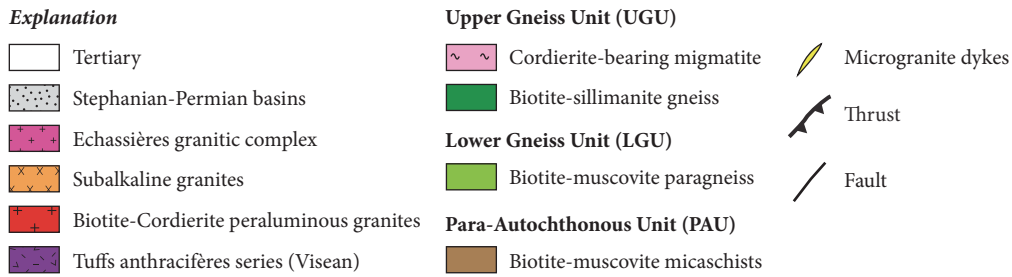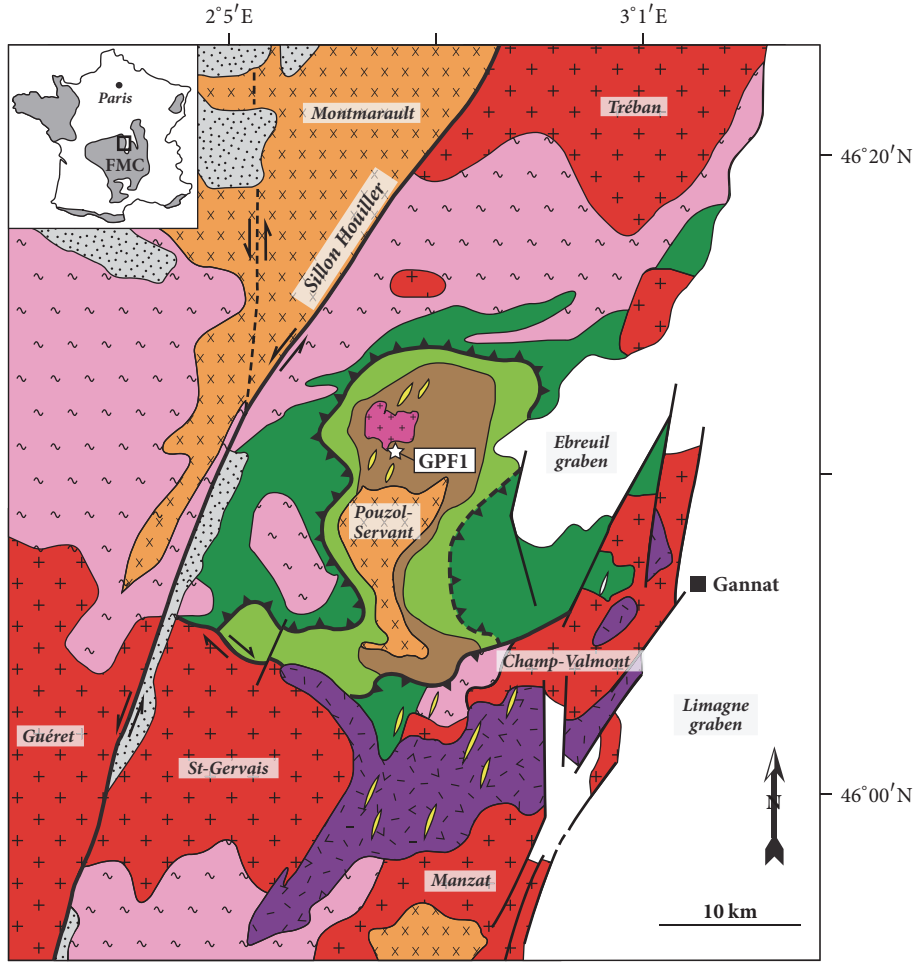
FIGURE 1: Geological setting of the Echassières granitic complex in the NE part of the French Massif Central (FMC) (modified from [11]). The location of the GPF1 drill hole from the "Géologie Profonde de la France" program is indicated.

evolution reflects the progressive increase in trace element contents (200–1,200 ppm Sn, 50–150 ppm Nb, 30–300 ppm Ta, 20–70 ppm W, 200–600 ppm Cs, 25–500 ppm Be, and 700–2,800 ppm Li) in whole-rock geochemistry that has been interpreted as a magmatic differentiation trend upward [12, 13]. The Echassières granitic complex, with an outcrop extension of ca. 40 km^2, was estimated from gravimetric data to be 3 to 4 km thick, with an overall volume of ca. 65 km^3 [37]. The Beauvoir granite, outcropping over 0.10 km^2, was estimated of a minimum volume of ca. 0.21 km^3 [13] and was emplaced as a sheet intruded into the micaschists and the Echassières granitic complex (Figure 2). Nowadays, the upper parts of the Beauvoir and Colettes granites are strongly kaolinized and are mined in open-pit quarry for kaolin by the company Imerys Ceramics France producing ~20 kt/yr of kaolin as well as ~60 t/yr of mineral concentrates of cassiterite, columbite-tantalite, and microlite as by-products.

The emplacement of the Beauvoir granite has been dated at 308±2 Ma, based on ^{40}Ar-^{39}Ar dating of lepidolite from the B1 facies [38]. However, a recent U-Pb dating of columbite-tantalite from the same facies yielded an age of 317 ± 6 Ma [10], which is slightly older than the previous age. This age
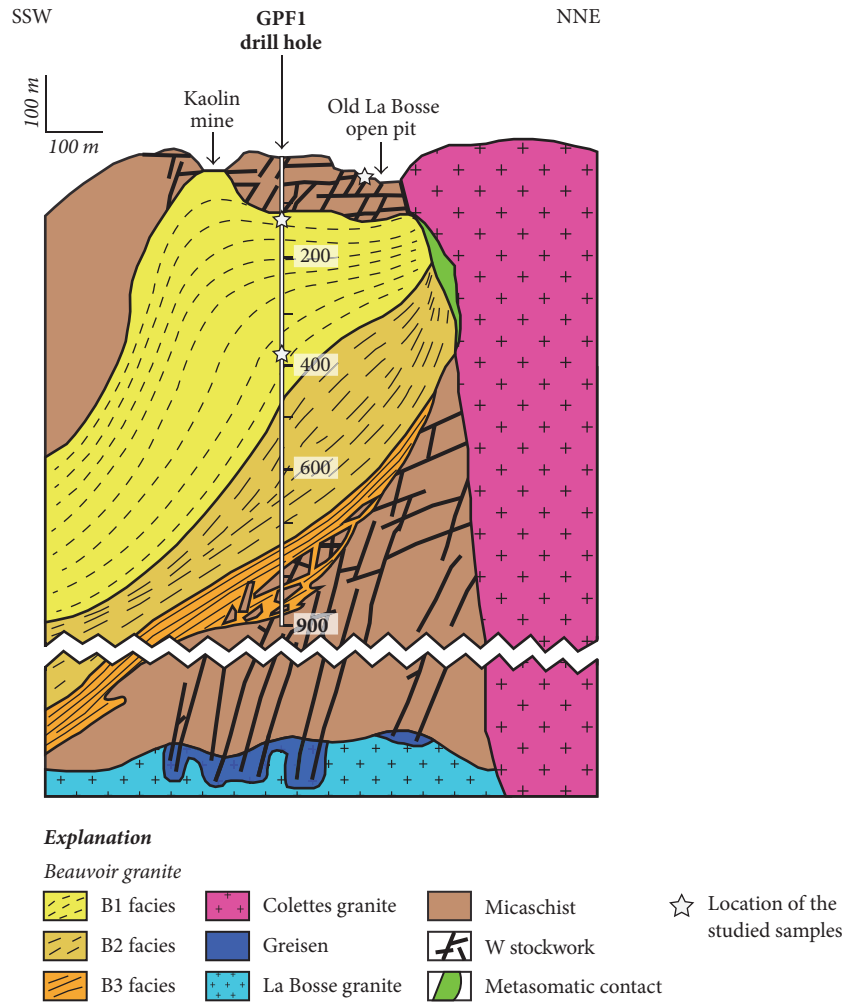
FIGURE 2: Interpretative cross-section of the Beauvoir granite from the GPF1 drill hole showing the vertical magmatic internal zoning composed by the three successive facies B1, B2, and B3 (modified from [12]). The location of the samples studied in this work is also reported.

discrepancy raises therefore the question of the reliability of the lepidolite age and the eventual existence of a perturbing thermal event, which could have partially reset the ^{40}Ar-^{39}Ar isotopic system of micas. Indeed, lepidolite is partly replaced by Li-muscovite in the B1 facies, which has been interpreted as a subsolidus fluid-rock interaction resulting from the mixing of the magmatic fluid exsolved from the granite with an external fluid at high temperature during the late stages of the Beauvoir granite emplacement [12]. There is no known high-temperature event after dating the emplacement of the Beauvoir granite, which could have reopened the ^{40}Ar-^{39}Ar isotopic system of micas. A series of lower temperature hydrothermal stages are described in the B1 granite [39], but the earliest event following the Li-muscovite alteration has been dated from the Upper Jurassic at 151 ± 4 Ma (K-Ar on illite [39]) and was too low in temperature ($T \leq 250°$C) to reset the ^{40}Ar-^{39}Ar isotopic system of micas. Therefore, the ^{40}Ar-^{39}Ar age obtained on lepidolite seems reliable and an emplacement age of ca. 310 Ma for the Beauvoir granite is

consistent within uncertainty with the two existing U-Pb and ^{40}Ar-^{39}Ar ages.

The La Bosse W stockwork consists in a network of up to 0.6 m-thick quartz-ferberite veins, which are hosted in the micaschists of the PAU and have been dated at 334 ± 2 Ma (U-Pb on wolframite [40]). The micaschists and the hosted W stockwork are crosscut by the Colettes and Beauvoir granites and were overprinted by the contact metamorphic aureole (Figure 3(a)). Aplites and pegmatites derived from the Beauvoir granite also crosscut the W stockwork (Figures 3(b) and 3(c)). There are two sets of veins, one subparallel and one oblique to the regional foliation, resulting from hydraulic fracturing (Figure 3(d)). Tungsten mineralization is polyphase at the vein scale, since three generations of quartz-ferberite veins have been recognized and emplaced by a crack-and-seal mechanism [41, 42]. The stockwork was strongly overprinted by the magmatic fluids issued from the Beauvoir granite, resulting in the crystallization of massive topaz ("topazite"), partial replacement of quartz in the veins,
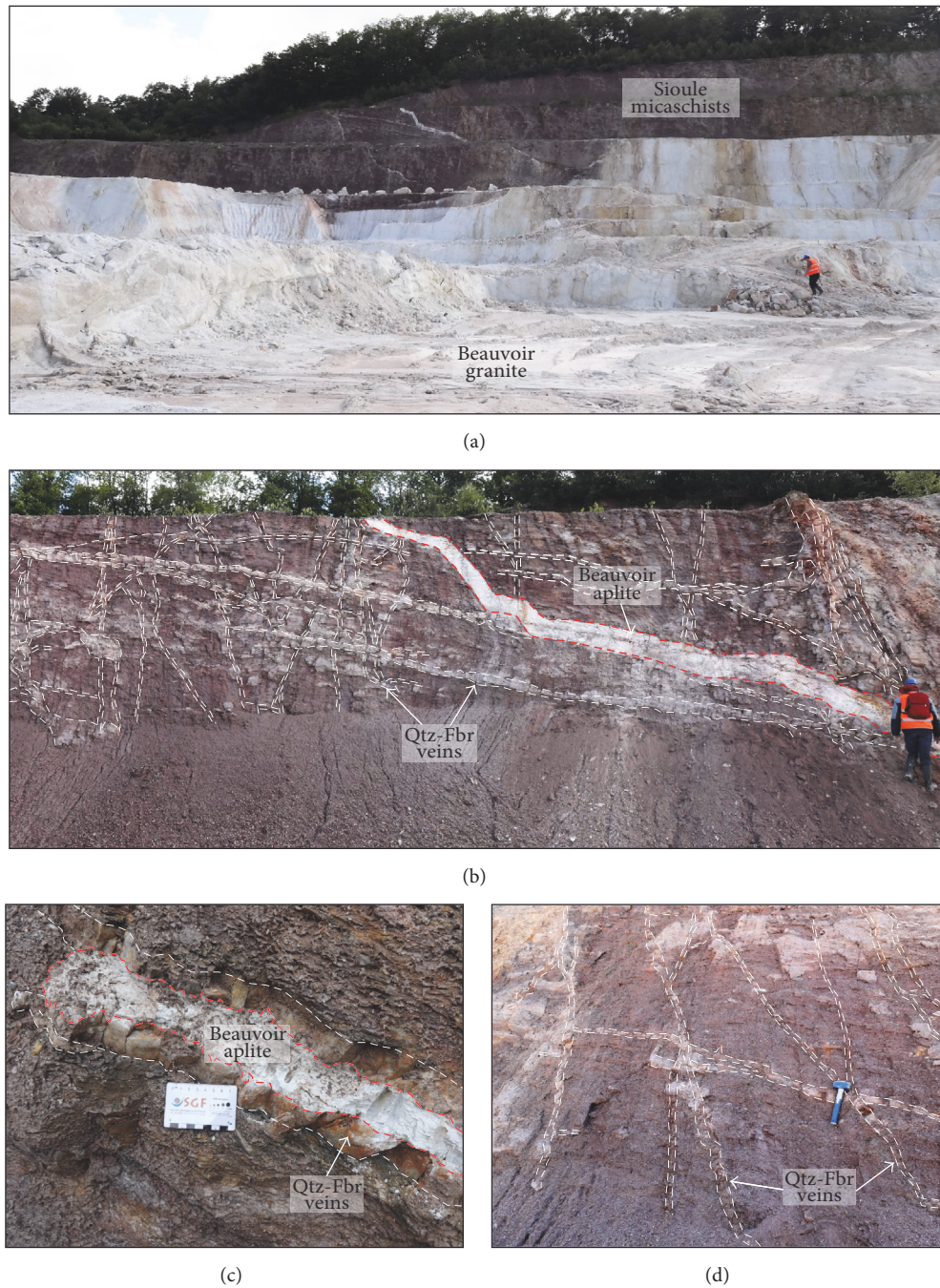
(a)

(b)

(c)

(d)

FIGURE 3: Field photographs of the Beauvoir granite and relationships with the enclosing micaschists. (a) General overview of the upper part of the kaolinized Beauvoir granite intrusive into the Sioule micaschists. (b) Aplite dyke derived from the roof of the Beauvoir granite that crosscut the preexisting quartz- (Qtz-) ferberite (Fbr) veins in the enclosing micaschists. (c) Detailed view of a Beauvoir aplitic dyke reopening an older quartz-ferberite vein. (d) Detailed view of the W stockwork showing the two sets of subparallel and oblique veins that crosscut the micaschists.

and crystallization of late Li-micas and Nb-Ta-W oxides [12]. Ferberite is weakly altered within the topazite, with the formation of dissolution microcavities associated with the sequential crystallization of Ta-rich ferberite, wolframoixiolite, and columbite-tantalite minerals [42]. The development of metasomatic topaz was also observed in the GPF1 drill hole, but only in the upper part of the stockwork located above the roof of the Beauvoir granite (<-100 m). Indeed, the quartz-ferberite veins in the micaschist enclaves found at the bottom of the drill hole (>-880 m) were devoid of any topaz [12]. Consequently, the metasomatic alteration appears as a halo located at the top of the B1 granitic cupola and structurally controlled by the preexisting quartz-ferberite stockwork, thus pointing to a quartz-undersaturated, F- and

Al-rich fluid and also enriched in rare-metals (W, Nb, Ta, and Li), which was likely derived from the Beauvoir granite.

2.3. Nature of the Fluid Circulations in the Beauvoir Granite.
Previous works on fluid inclusions in the Beauvoir granite system allowed to reconstruct the P-T-t conditions of fluid circulations and to determine the nature of the different fluid generations [12, 46]. (i) Early magmatic fluids (L1) were only found in topaz from the B1 facies and correspond to high-temperature (490–590°C) brines (25–30 wt.% NaCl eq), which are rich in Li as indicated by low eutectic temperatures ($T_e < -65$°C) and direct LIBS measurements (7,500–13,000 ppm Li [29]). The exsolution of this fluid is estimated at ca. 600°C and 0.8 kbars. (ii) Boiling of the L1 fluid occurred at high temperature (400–520°C) after a rapid decompression at ~0.7 kbars ("first boiling") and yielded by phase separation to a low- to moderate-salinity vapour (V2; 3–12 wt.% NaCl eq) and a high-salinity brine (L2; 30–50 wt.% NaCl eq). (iii) A low-salinity (2–6 wt.% NaCl eq) aqueous fluid (L3) found in the Beauvoir granite was trapped at lower temperature (330–420°C) and is interpreted from both microthermometric data [46] and stable isotopes data [12] to record the mixing between an external aqueous fluid and the magmatic brine L2 during the cooling of the granite. (iv) Later circulations involved several generations of aqueous fluids, including low-salinity fluids (L4a; 0–10 wt.% NaCl eq; 120–350°C), moderate-salinity brines (L4b; 20–26 wt.% NaCl eq; 200°C), and hypersalinity brines (L4c; 40–60 wt.% NaCl eq; 180–225°C). Fluid inclusions found in the topaz replacing the quartz-ferberite veins from the La Bosse stockwork correspond to the same L1, L2, and V2 fluids as in the Beauvoir granite [46]. The early fluid inclusions (L1, L2, and V2) trapped in the primary quartz and topaz from the granite and the stockwork were interpreted as the primary magmatic fluids exsolved from the B1 granite [12, 46] and are consequently the main target of the present study.

3. Materials and Analytical Methods

3.1. Studied Material.
The studied material come from two provenances: (i) two samples of the Beauvoir granite, which were taken from the GPF1 drilling core of the B1 facies at the depths −125 m (sample B1-125; Figure 4(a)) and −379 m (sample B1-379; Figure 4(b)). These samples allow studying fluid inclusions in the most evolved facies (B1) of the Beauvoir granite located at the top of the granitic cupola, where magmatic fluids are assumed to have been concentrated during the magmatic-hydrothermal transition; (ii) two samples of the metasomatized topaz-quartz-ferberite stockwork, which come from a surface sampling of the old La Bosse quarry, now inaccessible (samples ECH-X2 and ECH-11; Figures 4(c) and 4(d)). These samples allow studying the fluid inclusions in the overprinted vein system and their comparison with those found in the Beauvoir granite. Double-polished thick sections (150–200 μm thick) were prepared for microscopic observations of fluid inclusions in primary quartz and topaz crystals (Figure 5) using an Olympus BX51 optical microscope. Petrographic characterization of fluid inclusions was based on the criteria established by Roedder [47]. All analyses were performed at the GeoRessources laboratory (Université de Lorraine, Vandœuvre-lès-Nancy, France).

3.2. Microthermometry.
Microthermometric measurements were realized on a Linkam THMS600 heating-cooling stage connected to an Olympus BX51 microscope. This system allows measurements in a temperature range between −190°C and 600°C and is connected to a cooling circuit for measuring temperatures > 300°C. Calibration was done before each analytical session using H_2O synthetic capillaries and H_2O-CO_2 natural fluid inclusions standards. The accuracy of measurements varies from ±0.2°C at low temperature to ±2°C at high temperature. The following phase transition temperatures were measured during the microthermometric measurements: the eutectic temperature (T_e) corresponding to the first visible melting, that is, the apparition of the first visible liquid from the solidified aqueous phase during heating; the ice-melting temperature ($T_m$ice) corresponding to the final melting of solidified aqueous phase; the final melting temperature of hydrohalite (T_mHh); the final melting temperature of halite (T_mHl); and the total homogenization temperature (T_H), with occur to the liquid phase (L) or to the vapour phase (V). Most of these phase transition temperatures were determined using a heating-cooling cycling method to obtain precise measurements and to avoid metastability effects [48, 49]. Thick sections of the selected samples were observed under the optical microscope in order to select only fluid inclusions showing petrographic characteristics (content, shape, and size) of the primary fluid inclusions identified by Aïssa et al. [46]. The selected fluid inclusions were firstly investigated at high temperature during microthermometry in order to select only those with $T_H > 300$°C, which correspond in principle to the early magmatic fluid inclusions. A progressive step-heating procedure was conducted to limit fracturing of the host-mineral and decrepitation of fluid inclusions. Fluid inclusions were progressively heated with a temperature rate of 30°C/min between room temperature and 200°C, then 20°C/min for 200°C < T < 400°C, and finally 10°C/min for T > 400°C in order to estimate rapidly the temperature thresholds of the observable phase transitions. Then, the different phase transition temperatures (T_mHl, T_H) were precisely measured with a temperature rate of 1-2°C/min during a second heating cycle. Photographs of fluid inclusions after microthermometric measurements were then compared with the initial pictures before the experiments in order to evaluate any leakage, such as the presence of microcracks or visual variations in shape and/or volume of the vapour phase. The selected fluid inclusions were then analysed during cooling/freezing experiences. Fluid inclusions were firstly overcooled ($T < -100$°C) to freeze completely the aqueous and vapour phases and then the temperature of phases transitions (T_e, $T_m$ice, and T_mHh) were measured while progressively reheating with a temperature rate of 0.2–0.5°C/min typically.

3.3. Raman Spectrometry.
Fluid inclusions were analysed by Raman spectrometry using a Horiba Jobin-Yvon LabRAM spectrometer equipped with a 1800 gr mm^{-1} grating and an

(a) Beauvoir granite (*sample B1-125*)

(b) Beauvoir granite (*sample B1-379*)

(c) La Bosse stockwork (*sample ECH-X2*)
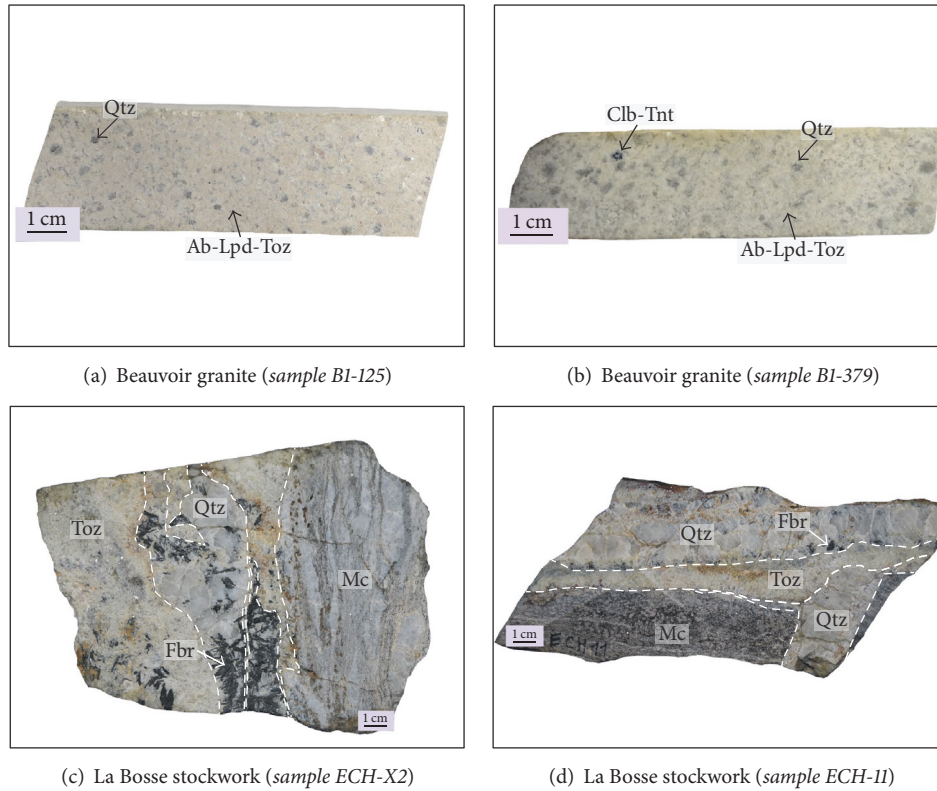

(d) La Bosse stockwork (*sample ECH-11*)

FIGURE 4: Photographs of the studied samples from the Beauvoir granite ((a), (b)) and the La Bosse stockwork ((c), (d)). Ab: albite; Clb-Tnt: columbite-tantalite; Fbr: ferberite; Lpd: lepidolite; Mc: micaschist; Qtz: quartz; Toz: topaz.

Edge filter. The confocal hole aperture is of 500 μm and the slit aperture is of 100 μm. The excitation beam is provided by a Stabilite 2017 Ar$^+$ laser (Spectra Physics, Newport Corporation) at 514.532 nm and a power of 400 mW, focused on the sample using ×50 and ×100 objectives equipped on an Olympus BX40 microscope. The laser beam diameter is around 1 μm. The signal-to-noise ratio was optimized ideally lower than 1% by adjusting the acquisition time and accumulation number. All Raman spectrometry analyses were done at room temperature. Salinity of the aqueous phase in fluid inclusions was estimated by following the method of Caumon et al. [45] and is expressed in wt.% NaCl eq. The uncertainty of the measurement is ±0.3 wt.% NaCl eq. The quantitative analysis of the gas composing the vapour phase within the fluid inclusions was determined using an in-house calibration. Results are expressed in mol% relative to the volatile phase. Finally, solids eventually present within the fluid inclusions were also identified when possible.

3.4. LA-ICPMS Analysis. Chemical composition of the fluid inclusions was determined by laser ablation-inductively coupled plasma mass spectrometry (LA-ICPMS) using an Agilent 7500c quadrupole ICPMS coupled with a 193 nm GeoLas ArF Excimer laser (MicroLas, Göttingen, Germany). Laser ablation was performed with a constant 10 Hz pulse frequency and a constant fluence of 7 J/cm^2 by focusing the beam at the sample surface in the ablation cell with a Schwarzschild objective and using a stepwise opening procedure [50], starting the ablation with a laser spot diameter of 2 μm and stepwise increasing the spot diameter to the size of the fluid inclusion (from 10 to 80 μm). This procedure allows a controlled ablation by reducing the mechanical stress on the mineral surface, which limits the risk of splashing of the fluid [50]. Helium was used as carrier gas to transport the laser-generated particles from the ablation cell to the ICPMS and argon was added as an auxiliary gas via a flow adapter before the ICP torch. Typical flow rates of 0.5 L/min for He and 0.87 L/min for Ar were used. The certified reference material NIST SRM 610 (concentrations from [51]) was used as external standard for calibration of all analyses and was analysed twice at the beginning and at the end for each set of samples, following a bracketing standardization procedure. The reference material NIST SRM 612 was also used as control standard to control the analytical conditions (in particular accuracy and precision). LA-ICPMS calibration was optimized for highest sensitivity on an intermediate m/Q range, while maintaining Th/U ~ 1 and ThO/Th < 0.5%, as determined on NIST SRM 610. The following isotopes were measured with a total cycle time of 350 ms: ^{7}Li, ^{23}Na, ^{24}Mg, ^{29}Si, ^{39}K, ^{44}Ca, ^{55}Mn, and ^{57}Fe with a dwell time of 10 ms; ^{85}Rb and ^{88}Sr with a dwell time of 35 ms; ^{93}Nb, ^{118}Sn, ^{133}Cs, ^{181}Ta, and ^{182}W with a dwell time of 40 ms. Data reduction

(a) Beauvoir granite (*sample B1-125*)

(b) Beauvoir granite (*sample B1-379*)

(c) La Bosse stockwork (*sample ECH-X2*)

(d) La Bosse stockwork (*sample ECH-11*)

(e) Beauvoir granite (*sample B1-125b*)
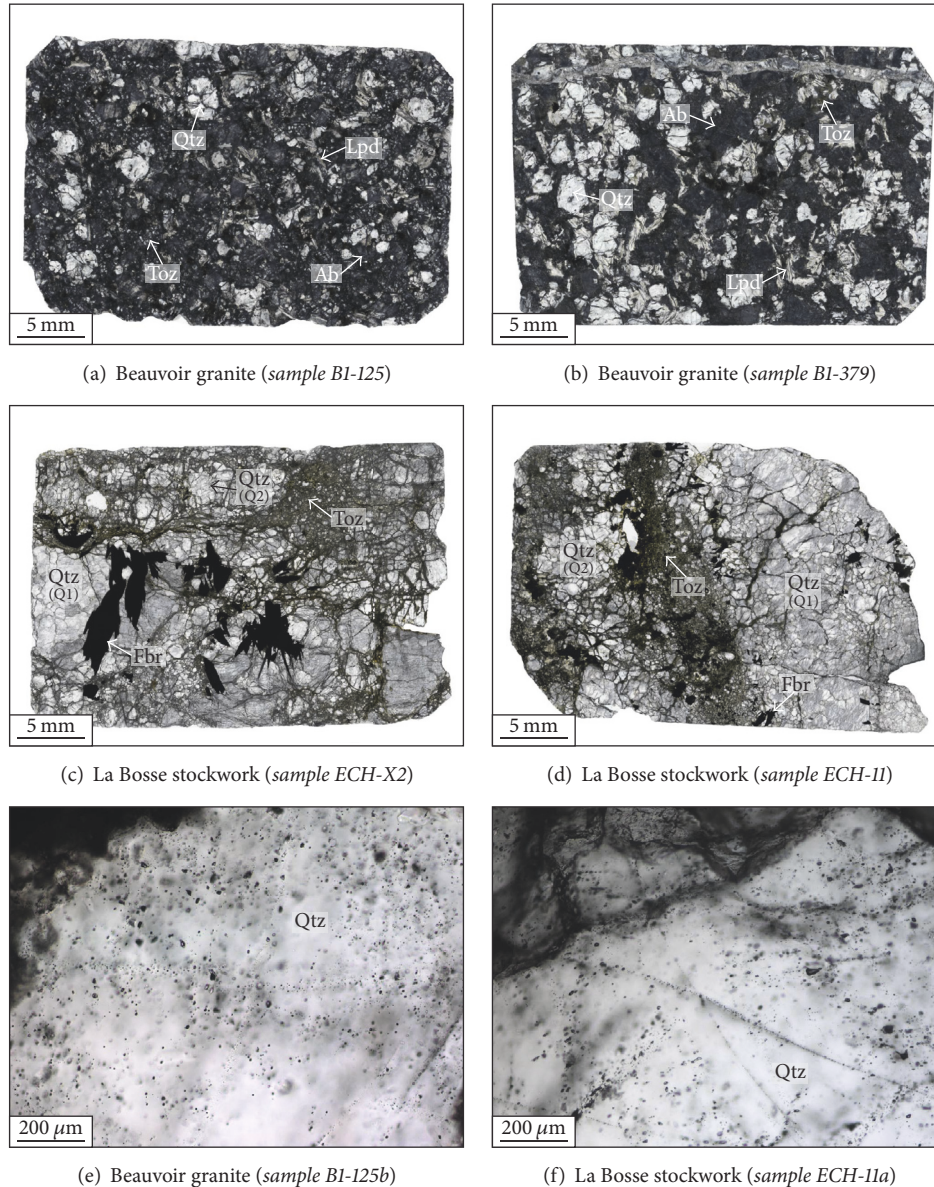

(f) La Bosse stockwork (*sample ECH-11a*)

FIGURE 5: Photographs of thick sections of the studied samples from the Beauvoir granite ((a), (b)) and the La Bosse stockwork ((c), (d)). Representative microphotographs of fluid inclusions observed in primary quartz from the Beauvoir granite (e) and the La Bosse stockwork (f) are shown. Note the density of disseminated fluid inclusions within the primary quartz and the presence of secondary fluid inclusions planes. Ab: albite; Fbr: ferberite; Lpd: lepidolite; Qtz: quartz; Toz: topaz.

and absolute quantification of signals were performed using the software StalQuant, developed at ETH Zürich, Switzerland (see details in [52]). For all analyses, ^{23}Na was used as internal standard for calculation of absolute concentrations. The molality of Na (in mol/kg) was calculated from the NaCl content (in wt.% eq) of the aqueous phase in fluid inclusions determined by Raman spectrometry when measured and/or from the microthermometric data, following a charge-balancing method to an estimated chloride concentration [53]. Limits of detection (LOD) were calculated using the 2σ criterion detailed in Longerich et al. [54].

4. Results

4.1. Fluid Inclusion Petrography. Fluid inclusions were described at room temperature under the optical microscope according to their distribution, size, shape, number of visible phases, and volumic fraction of the vapour phase (Rv%). Four main types of fluid inclusions (L1, L2, V2, and L3) were identified in quartz and topaz crystals from the Beauvoir granite and the La Bosse stockwork by petrographic and microthermometric studies, in accordance with the previous results from Aïssa et al. [46]. The characteristics of the studied fluid inclusions are summarized in Table 1.

Geofluids

9

TABLE 1: Petrography, microthermometry, and Raman spectrometry data for the different fluid inclusion types from the Beauvoir granite and the La Bosse stockwork.

| FI-type | Petrography | | | Microthermometry | | | | | Bulk salinity | | Gas composition (mol%) | | | |
	n	Rv (%)	Size (μm)	T_e (°C)	$T_m$ice (°C)	T_mHh (°C)	T_mHl (°C)	T_H (°C)	wt.% NaCl eq	n	CO_2	N_2	CH_4	H_2S
Beauvoir granite														
L1-type	11	20; 60; 40	10–23	−78; −56; −73	−39.9; −12.8	−44	275; 300; 287	491; >600; 542	16.7; 28.1; 26	7	9.7; 65.6; 43.8	20; 81.8; 46	0.3; 22.2; 10.2	—
V2-type	4	80; 90; 90	12–24	−72	−19.3	—	300	375; 595; 465	4.7; 21.9; 15.3	3	57.5; 60.1; 58.5	31.5; 35.2; 33.7	7.2; 8.4; 7.8	—
L2-type	13	20; 40; 30	10–35	−77; −52	−39.9; −1.6	—	215; 407; 359	377; 542; 455	32.6; 48.2; 43.6	1	52.4	34.3	13.2	—
L3-type	1	40	16	−61	−4.26	—	—	322	6.8	—	—	—	—	—
La Bosse stockwork														
L1-type	3	40; 40; 40	10–24	−80	−30; −8	−48.7	—	377; 468; 422	27; 28.7; 28	—	—	—	—	—
V2-type	16	60; 80; 60	15–47	−65	−6; −1.4; −3.5	—	—	342; 490; 403	1.4; 9.2; 4.5	7	38.6; 84.3; 55.7	12.9; 53.6; 36.6	2.4; 12.5; 5.9	0; 6.3; 1.7
L2-type	14	30; 40; 30	16–30	−81; −60	−41.8; −2.5	—	263; 328; 286	305; 439; 375	36.7; 40.4; 37.3	—	—	—	—	—
L3-type	27	10; 70; 40	10–77	−72; −61; −72	−2.9; −0.15; −2.1	—	—	338; 398; 380	1.5; 6.5; 3.7	13	22.6; 87.9; 58	7.7; 73.9; 36	0; 10.5; 5.9	—

Values indicated correspond, respectively, to the minimum, maximum, and mode values. Mean values are indicated in italics; —: not determined.

(a) L1-type (*sample B1-379a*)

(b) V2-type (*sample B1-379a*)

(c) L2-type (*sample B1-379a*)

(d) V2-type (*sample ECH-11a*)

(e) L2-type (*sample ECH-X2b*)

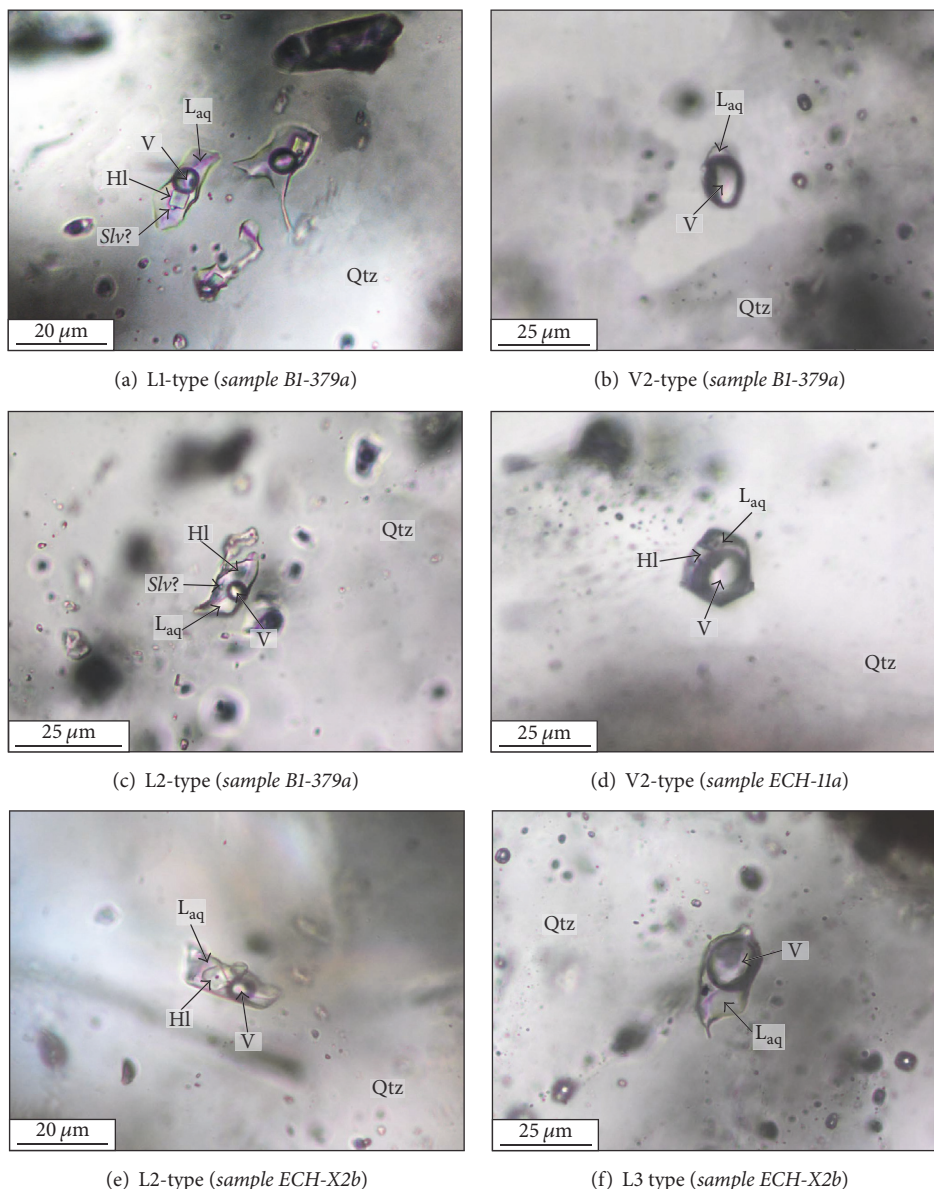(f) L3 type (*sample ECH-X2b*)

FIGURE 6: Microphotographs showing the different types of fluid inclusions. Detailed description of each fluid inclusion type is given in the text. (a) L1-type fluid inclusion in globular quartz crystal from the Beauvoir granite. (b) V2-type fluid inclusion disseminated in globular quartz from the Beauvoir granite. (c) L2-type fluid inclusion from a globular quartz crystal in the Beauvoir granite. (d) V2-type fluid inclusion isolated in the limpid quartz (Q2) from the La Bosse stockwork. (e) L2-type fluid inclusion in limpid quartz (Q2) from the La Bosse stockwork. (f) L3-type fluid inclusion disseminated in limpid quartz (Q2) from the La Bosse stockwork. Hl: halite; L_{aq}: liquid aqueous phase; Qtz: quartz; Slv: sylvite; V: vapour phase.

4.1.1. Fluid Inclusions in the Beauvoir Granite.

In the Beauvoir granite (facies B1; Figures 5(a) and 5(b)), the quartz forms anhedral to euhedral millimetric globular magmatic crystals, which contain many fluid inclusions. Topaz forms generally limpid subeuhedral crystals disseminated into the granite and contain less fluid inclusions than the quartz. The fluid inclusions in the quartz and topaz crystals form dense clouds of disseminated fluid inclusions or secondary planes (Figure 5(e)). This represents a severe limitation to the identification of the different generations of fluid inclusions based on criteria of relative position or arrangement.

Nevertheless, four main types of fluid inclusions can be distinguished in quartz and topaz based on petrography and microthermometry results.

(i) L1-Type Fluid Inclusions. These are generally found in clusters within the quartz and topaz and have irregular shapes with a size typically ranging from 10 to 23 μm. These consist of multiphase (liquid + vapour + solid) fluid inclusions at room temperature, with a dominant aqueous phase containing a vapour bubble (Rv = 40% on average) and small (<5 μm) isotropic solids, including halite and possibly sylvite (Figure 6(a)).

(ii) V2-Type Fluid Inclusions. These consist of two-phase (liquid + vapour) irregularly shaped inclusions disseminated in clusters, which are independent of the L1 clusters. They contain a dominant vapour phase (Rv > 80%) and range approximately from 12 to 24 μm in size. Small cubic or rounded crystals of salts (most likely halite) are occasionally observed (Figure 6(b)).

(iii) L2-Type Fluid Inclusions. These are characterized by irregular to regular shapes and have typical sizes comprised between 10 and 35 μm. They consist of multiphase (liquid + vapour + solid) fluid inclusions, disseminated in clusters in the quartz and topaz. These clusters are independent of the L1 and V2 clusters. The L2-type fluid inclusions contain a dominant aqueous phase and a small vapour phase (Rv = 30% on average) and contain several ($n > 2$) crystals of salts, including halite and possibly sylvite (Figure 6(c)).

(iv) L3-Type Fluid Inclusions. They consist of regularly shaped two-phase (liquid + vapour) fluid inclusions of moderate size (15–20 μm), which contain a small vapour bubble (Rv ∼ 40%). They are less numerous in the granite and are found as clusters or isolated fluid inclusions, without any clear spatial relationships with the other fluid inclusions types.

4.1.2. Fluid Inclusions in the La Bosse Stockwork. Two types of quartz can be distinguished in the topaz-quartz-ferberite-veins samples from the La Bosse stockwork (Figures 5(c) and 5(d)). Grey quartz (Q1) forms large crystals and contains numerous and small (<10 μm) fluid inclusions, either disseminated or forming intragranular planes. The Q1 quartz is deformed and the fluid inclusions appear as black decrepitated or deformed inclusions, probably due to the thermal effect of the Colettes granite emplacement [46]. Based on these observations, Q1 is interpreted as the primary quartz from the quartz-ferberite veins and was not considered in the present study. A limpid quartz (Q2) is also observed that appears as small interstitial crystals or as vein infillings within the altered quartz-ferberite veins. This second generation of quartz is intergrown with topaz and is therefore interpreted as formed by the magmatic fluids from the Beauvoir granite. Fluid inclusions encountered in either Q2 or in topaz are found as disseminated clusters or intragranular planes (Figure 5(f)) and correspond to the same types of fluid inclusions as those found in the granite.

(i) L1-Type Fluid Inclusions. These were found in the Q2 quartz from the stockwork, but not in topaz, being significantly less frequent than in the granite samples. They consist of multiphase (liquid + vapour + halite) fluid inclusions with very irregular shapes, ranging from 10 to 24 μm in size.

(ii) V2-Type Fluid Inclusions. They are more frequent in the Q2 quartz and topaz of the stockwork samples than in the Beauvoir granite. They are characterized by regular to slightly irregular shapes with sizes ranging from 15 to 50 μm and are always found isolated or in clusters (Figure 6(d)). They contain a dominant vapour phase (Rv ∼ 60%) with small (<5 μm) greenish elongated isotropic solids observed occasionally and identified as halite.

(iii) L2-Type Fluid Inclusions. These have variable sizes (16–30 μm) with a dominant aqueous phase and a small vapour bubble (Rv ∼ 30% on average) and contain several ($n = 1$–3) small isotropic solids including halite (Figure 6(e)).

(iv) L3-Type Fluid Inclusions. They are by far the most abundant fluid inclusions within the Q2 quartz and topaz crystals from the stockwork. They consist of two-phase (liquid + vapour) fluid inclusions with a small vapour bubble (Rv ∼ 20–40%), which are irregular to very regular in shape and range from 10 to 77 μm in size (Figure 6(f)).

4.2. Microthermometry and Raman Spectrometry Results. Microthermometric and Raman spectrometry data for the different fluid inclusions analysed are given in Table 1 and Figure 7. Despite the use of a careful step-heating procedure, the T_H measurements were strongly limited by the decrepitation of many fluid inclusions (ca. 75%) before bulk homogenization, which represent therefore a severe limitation for the acquisition of statistics data. The decrepitation temperatures range from 250 to 500°C with a mode at ca. 400°C. Globally, the new results reproduce well the earlier findings of Aïssa et al. [46], including the systematic ΔT of ∼100°C, which is observed between the T_H measurements in the Beauvoir granite, on the one hand, and in the La Bosse stockwork, on the other hand, for the same type of fluid inclusions.

4.2.1. L1-Type Fluid Inclusions. These are characterized by very low eutectic temperatures (−80°C < T_e < −56°C) and very low ice-melting temperatures (−39.9°C < $T_m$ice < −12.8°C). Hydrohalite melting was observed only in two fluid inclusions between −48.7 and −44°C. Most of the solids observed within the fluid inclusions correspond to halite crystals. Halite melting occurred in the Beauvoir granite between 275 and 300°C before the total homogenization, with an average value of 287°C. One crystal of cassiterite (ca. 2 μm in size) was identified by Raman spectrometry within one fluid inclusion hosted in a topaz crystal from the Beauvoir granite (sample B1-379c, FI n°6a; Figure 8) and did not disappear during heating. In the Beauvoir granite, T_H (L) range from 491 to >600°C with an average value of 542°C. One fluid inclusion in a quartz crystal from the granite was not homogenized at 600°C, which is the upper limit of the Linkam stage used. Although no clathrate melting was observed in these fluid inclusions, which are mainly aqueous, the vapour phase contains very low-density volatiles, with dominant CO_2 (9.7–65.6 mol%) and N_2 (20–82 mol%) and minor CH_4 (0.3–22 mol%) (Figure 7; Table 1). In the La Bosse stockwork, T_H (L) are lower and range from 377 to 468°C with an average value of 422°C.

4.2.2. V2-Type Fluid Inclusions. These fluid inclusions have very low eutectic temperatures (−72°C < T_e < −65°C) and low ice-melting temperatures (−19.3°C < $T_m$ice < −1.4°C). One T_mHl was measured at 300°C in a V2 fluid inclusion from the granite, occurring before total homogenization. In the Beauvoir granite, the T_H (V) ranges from 375 to 595°C with an average temperature of 465°C. In the La Bosse stockwork, they range from 342 to 490°C with an
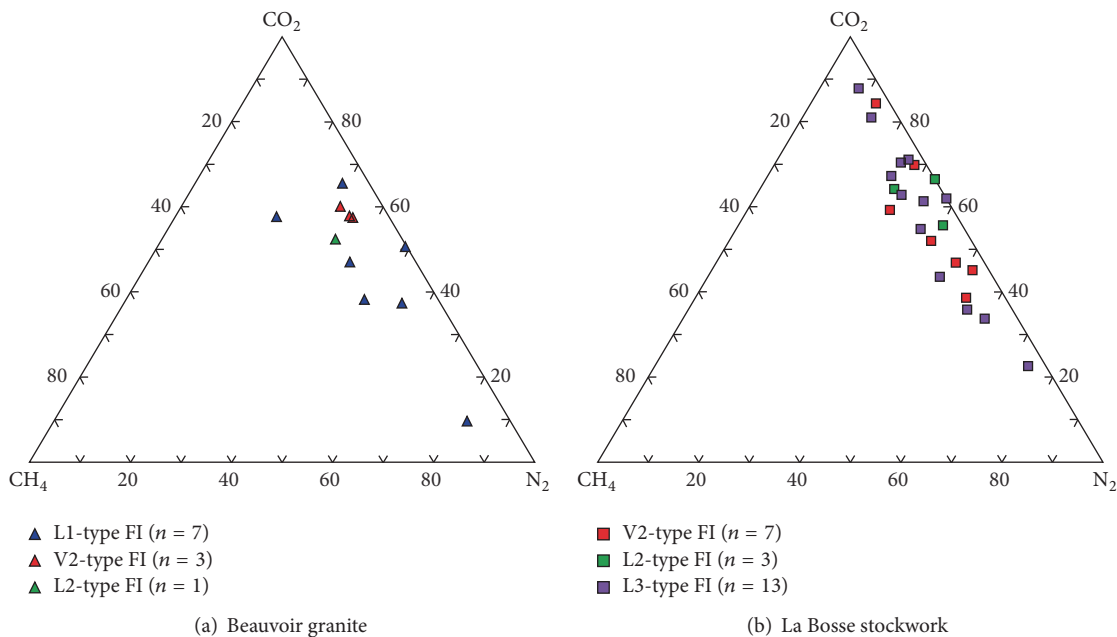
(a) Beauvoir granite

(b) La Bosse stockwork

FIGURE 7: Ternary diagrams CO_2-CH_4-N_2 showing the gas compositions of fluid inclusions from the Beauvoir granite (a) and the La Bosse stockwork (b) determined by Raman spectrometry. Representative Raman data of the different fluid inclusions analysed are given in Table 1.
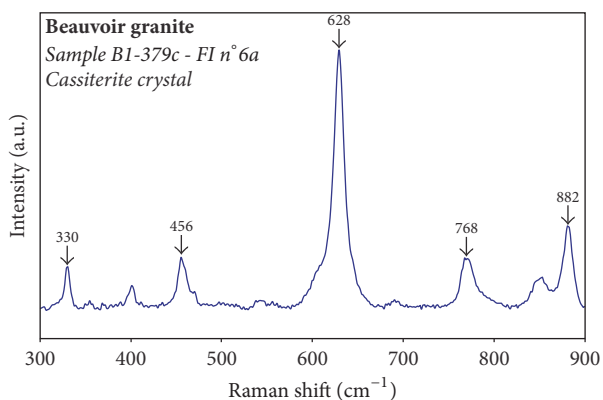

FIGURE 8: Raman spectrum of a cassiterite crystal contained in a primary L1-type fluid inclusion within a magmatic quartz crystal of the Beauvoir granite (sample B1-379c, FI n°6a). The Raman shift values indicated on the spectrum correspond to the Raman peaks of cassiterite. The other peaks are those of the host-quartz.

average temperature of 403°C. Total homogenization occurs mostly to the vapour phase, although a few fluid inclusions ($n = 6$) homogenized in supercritical phase. The vapour phase is dominantly composed by CO_2 (38.6–84.3 mol%), N_2 (12.9–53.6 mol%), and minor CH_4 (2.4–12.5 mol%) (Figure 7; Table 1). Minor H_2S (1.7 mol% on average) was detected in V2-type fluid inclusions from the stockwork. These fluid inclusions represent thus low-density fluids, which are composed in majority by vapour H_2O with trace contents of volatiles compounds (CO_2, N_2, and CH_4).

4.2.3. L2-Type Fluid Inclusions. These fluid inclusions have very low eutectic temperatures ($-81°C < T_e < -52°C$) and

very low ice-melting temperatures ($-41.8°C < T_m\text{ice} < -29°C$). Hydrohalite peritectic melting could not be observed in these fluid inclusions. Halite melting occurs systematically before total homogenization with $T_m\text{Hl}$ comprised between 215 and 407°C, with average values of 359°C in the Beauvoir granite and 286°C in the La Bosse stockwork. In the Beauvoir granite, T_H (L) ranges from 377 to 542°C with an average value of 455°C, whereas they range from 305 to 439°C with an average temperature of 375°C in the La Bosse stockwork. No clathrate melting was observed. The vapour phase is composed by CO_2 (52.4–66.5 mol%) and N_2 (34.3–40.5 mol%), with minor CH_4 (9.2–13.2 mol%) (Figure 7; Table 1).

4.2.4. L3-Type Fluid Inclusions. They have very low eutectic temperatures ($-72°C < T_e < -61°C$) and low ice-melting temperatures ($-4.3°C < T_m\text{ice} < -1.2°C$). T_H ranges from 338 to 398°C with an average temperature of 380°C in the La Bosse stockwork. Within the Beauvoir granite, only one T_H of 322°C could be measured. The vapour bubble corresponds to a low-density phase composed dominantly by CO_2 (22.6–87.9 mol%) and N_2 (7.7–73.9 mol%), with minor CH_4 (0–10.5 mol%) (Figure 7; Table 1).

4.3. Salinity Calculation. Salinity of the fluid inclusions can be estimated in two ways: (i) from the microthermometric data by knowing the nature of the cations-dominated chemical system, which can be determined by the measurement of T_e and by using experimentally known model systems, such as H_2O-NaCl or H_2O-NaCl-$CaCl_2$ ([43] and references therein), or (ii) from the Raman spectrometry analysis of the aqueous phase, which allows estimating the chlorinity with a similar precision to the microthermometry [45]. Both methods were used in the present study. The calculation of
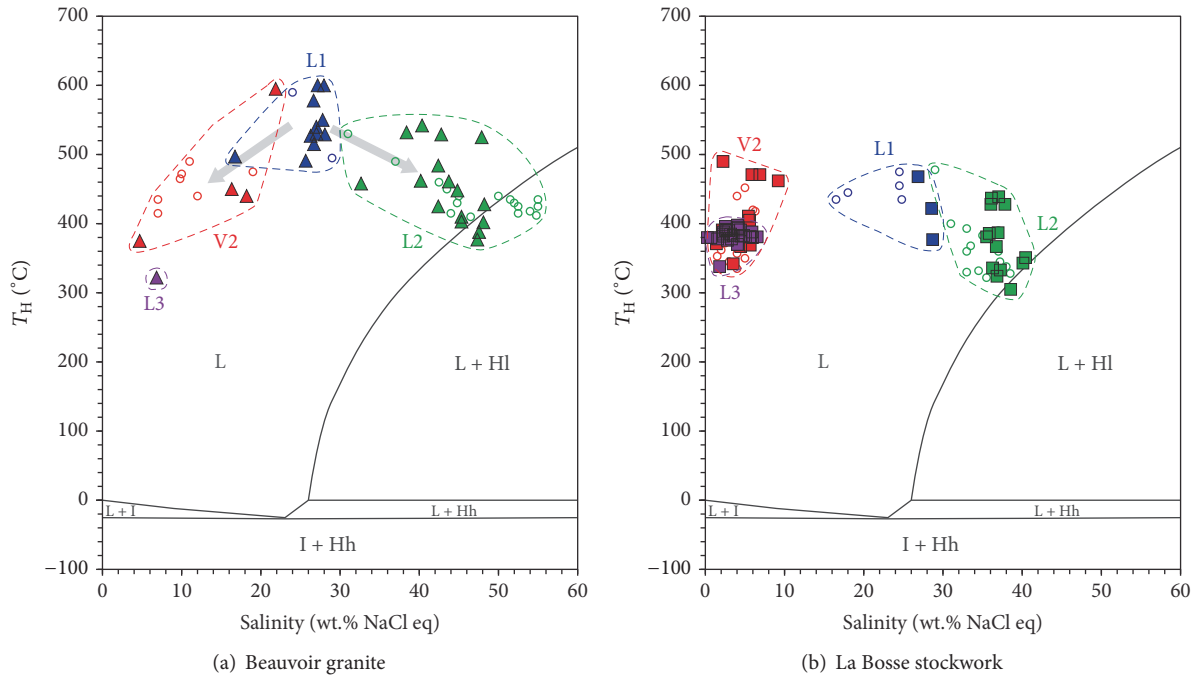
(a) Beauvoir granite

(b) La Bosse stockwork

FIGURE 9: Salinity versus T_H diagram for the different generations of fluid inclusions from the Beauvoir granite (a) and the La Bosse stockwork (b) studied in this work (filled symbols) and compiled with the previous data (open circles) from Aïssa et al. [46]. Data are given in Table 1. Phase equilibrium curves for the pure H_2O-NaCl system [43] are reported. L = liquid; Hl = halite; Hh = hydrohalite; I = ice.

the salinity for the different fluid inclusion types is explained below and a summary of the values is reported in Table 1. Final microthermometric data are shown hereafter in the salinity versus T_H diagram for the Beauvoir granite and the La Bosse stockwork (Figure 9).

4.3.1. Estimation of the Salinity from the Microthermometric Data. All the fluid inclusions analysed display very low eutectic temperatures ($-80°C < T_e < -60°C$) with a mode value at $-70°C$, which are typical of the H_2O-NaCl-LiCl system [44, 55]. In this system, the bulk salinity and the Na/Li ratio of the fluid can be estimated from the $T_m$ice, T_mHh, and T_mHl measurements [44]. However, the isotherms for temperatures > 100°C in the stability field of halite in the H_2O-NaCl-LiCl system are essentially not known at present, hindering in principle these estimations. It is however possible to partly overcome this difficulty by drawing hypothetical isotherms based on the comparison between the existing isotherms in the H_2O-NaCl-LiCl system [44] and those in the H_2O-NaCl-$CaCl_2$ system, which are known for temperatures up to 500°C ([43] and references therein). The extrapolation of isotherms in the H_2O-NaCl-LiCl diagram from the more known H_2O-NaCl-$CaCl_2$ diagram can be justified by the fact that these two thermodynamic systems have very similar invariant points (i.e., eutectic, peritectic; see [44]). This procedure allows estimating both Na/Li ratios and bulk salinity and was adopted for the fluid inclusions measured by microthermometry. The extrapolated H_2O-NaCl-LiCl ternary diagram is shown on Figure 10 and the
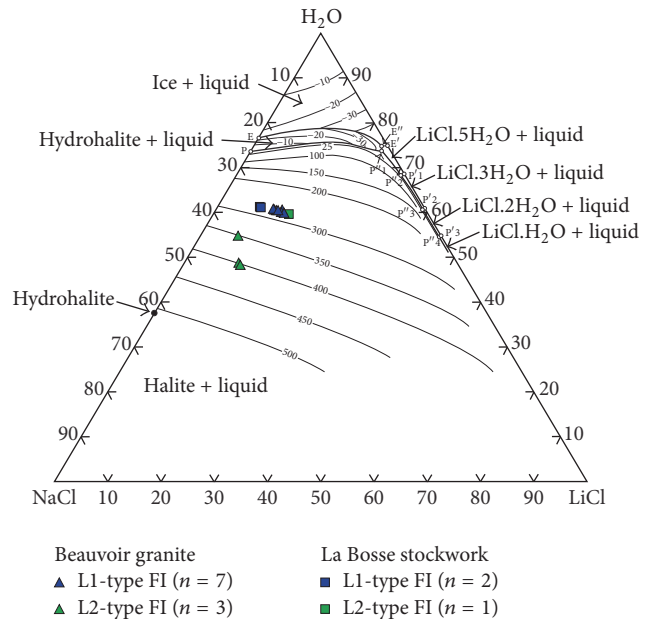
FIGURE 10: Phase diagram of the H_2O-NaCl-LiCl system (after [44]) in which the microthermometric data of the L1- and L2-type fluid inclusions are reported. Concentrations are expressed in wt.%. E, E′, and E″ refer to the eutectic points and P, P′, and P″ refer to the peritectic points (values given in [44]). Isotherms are given in °C and were extrapolated for $T > 100°C$ in the stability field of halite from the isotherms of the H_2O-NaCl-$CaCl_2$ diagram from Bodnar [43] (see explanation in text). Estimations of the bulk salinity and Na/Li ratios for the different fluid inclusions are reported in Table 2.

results are reported in Table 2 and were also compared with the salinity estimates obtained by using the simple H_2O-NaCl system [43].

For the L1-type halite-bearing fluid inclusions, the salinity was estimated from the $T_m$ice and T_mHl measurements (Figure 10). Only two T_mHl were measured precisely for these fluid inclusions at ca. 280°C (Table 2), due to the small size of the fluid inclusions in general (<15 μm on average). Based on the very similar T_mHl and considering that the measured T_mHh are equivalent, we assumed T_mHl value of 280°C for the other L1-type fluid inclusions measured, for which the halite disappearance was not clearly observed during heating. Bulk salinity calculated ranges from 24.9 to 28.5 wt.% NaCl eq and the Na/Li ratios are comprised between 4.6 and 6.5 for the L1-type fluid inclusions from the Beauvoir granite ($n = 7$). In the La Bosse stockwork, bulk salinity is estimated for the L1-type fluid inclusions ($n = 2$) from 30.8 to 31.6 wt.% NaCl eq with Na/Li ratios ~9. For the L2-type halite-bearing fluid inclusions, $T_m$ice and T_mHl measurements were also used and reported in the H_2O-NaCl-LiCl ternary diagram (Figure 10). In the Beauvoir granite, the T_mHl for the L2-type fluid inclusions are higher compared to those of the L1-type ones ranging from 354 to 406°C. Bulk salinity determined for L2-type fluid inclusions in the Beauvoir granite ($n = 3$) ranges from 37.8 to 41.9 wt.% NaCl eq with Na/Li ratios comprised between 9 and 12.6. For the La Bosse stockwork, one L2-type fluid inclusion is characterized by bulk salinity of 25.6 wt.% NaCl eq with a Na/Li ratio of 4.3. A rough estimation by simply using the H_2O-NaCl system [43] yields to salinity in the range of 31.9–36.8 and 42.8–48.1 wt.% NaCl eq for the L1- and L2-types fluid inclusions in the Beauvoir granite, respectively (Table 2), which seems overestimated.

Finally, for the two-phase (liquid + vapour) V2- and L3-types fluid inclusions, estimation of the salinity in the H_2O-NaCl-LiCl system requires the measurements of the $T_m$ice and T_mHh. However, it was not possible to observe the hydrohalite melting in these fluid inclusions, principally because of their small size (<15 μm on average), and therefore the salinity cannot be estimated directly in the H_2O-NaCl-LiCl system and was only estimated by Raman spectrometry when measured (see below) or calculated in the H_2O-NaCl system based on the $T_m$ice measurement, as the best possible approximation. The Na/Li ratios for the V2- and L3-types fluid inclusions were calculated from the LA-ICPMS analyses only.

4.3.2. Estimation of the Salinity from the Raman Spectrometry Data.

Considering the problem of T_mHl and T_mHh measurements, the Raman spectrometry represents an interesting alternative to estimate the bulk salinity of the fluid inclusions with a fast, systematic, and reproducible acquisition with accuracy better than ±10% on average [45]. The method developed by Caumon et al. [45] has been calibrated only for NaCl solutions, which may possibly lead to a bias in the salinity estimation of LiCl-rich fluid inclusions due to the deformation of the stretching band of water induced by Li. Nevertheless, previous study by Dubessy et al. [56] has shown that the Raman calibration curve for LiCl solutions is similar to the one of $CaCl_2$, both differing slightly from the

calibration curve of NaCl. Consequently, the salinity of the aqueous phase in fluid inclusions estimated by following the method of Caumon et al. [45] can be considered as a good approximation of the bulk salinity in the case of H_2O-NaCl-LiCl solutions. Salinity calculated by Raman spectrometry is reported in Table 3.

The estimated salinity for the L1-type fluid inclusions in the Beauvoir granite ranges from 25.7 to 28.1 wt.% NaCl eq, with an average of 27 wt.% NaCl eq ($n = 7$). One L1-type fluid inclusion from the La Bosse stockwork was measured by Raman spectrometry and yielded to a bulk salinity of 27 wt.% NaCl eq. The calculated salinity for the V2-type fluid inclusions ranges from 4.7 to 18.2 wt.% NaCl eq in the Beauvoir granite, with an average value of 13.1 wt.% NaCl eq ($n = 3$), and from 1.4 to 6.9 wt.% NaCl eq in the La Bosse stockwork, with an average value of 3.9 wt.% NaCl eq ($n = 6$). The Raman salinity was determined for one L2-type fluid inclusion in the La Bosse stockwork with a value of 37.6 wt.% NaCl eq. Salinity for L3-type fluid inclusions in the La Bosse stockwork ranges from 2.3 to 6.6 wt.% NaCl eq with an average value of 4.8 wt.% NaCl eq ($n = 10$).

4.3.3. Synthesis: Bulk Salinity of the Fluid Inclusions.

In conclusion, the salinity determined by Raman spectrometry is in good agreement with the one determined in the H_2O-NaCl-LiCl system, whereas the salinity determined in the H_2O-NaCl system appears overestimated in comparison with the two other calculated salinities. Therefore, the salinity determined by Raman spectrometry was used when measured, and if not, the salinity determined using the H_2O-NaCl-LiCl system was chosen. The final bulk salinity of the different type of fluid inclusions is shown in Table 1 and summarized below.

(i) L1-Type Fluid Inclusions. They have salinity comprised between 16.7 and 28.1 wt.% NaCl eq in the Beauvoir granite, with an average value of 26 wt.% NaCl eq, and between 27 and 28.7 wt.% NaCl eq in the La Bosse stockwork, with an average value of 28 wt.% NaCl eq.

(ii) V2-Type Fluid Inclusions. These have salinity ranging from 4.7 to 21.9 wt.% NaCl eq with an average value of 15.3 wt.% NaCl eq in the Beauvoir granite and from 1.4 to 9.2 wt.% NaCl eq in the La Bosse stockwork, with an average salinity of 4.5 wt.% NaCl eq.

(iii) L2-Type Fluid Inclusions. They are characterized by the highest salinities comprised between 32.6 and 48.2 wt.% NaCl eq in the Beauvoir granite, with an average of 43.6 wt.% NaCl eq, and between 36.7 and 40.4 wt.% NaCl eq in the La Bosse stockwork, with an average value of 37.3 wt.% NaCl eq.

(iv) L3-Type Fluid Inclusions. These have the lowest salinities in all the studied fluid inclusions. The only L3-type fluid inclusion analysed in the Beauvoir granite has a salinity of 6.8 wt.% NaCl eq, whereas they range from 1.5 to 6.5 wt.% NaCl eq in the La Bosse stockwork, with an average value of 3.7 wt.% NaCl eq.

TABLE 2: Salinity calculated from microthermometric data for the L1- and L2-types fluid inclusions in the H_2O-NaCl system [43] and H_2O-NaCl-LiCl system [44].

FI-type	Sample	FI n°	Host-mineral	Size μm	T_e °C	$T_m$ice °C	T_mHl °C	T_H °C	[NaCl] (1) wt.% eq	[NaCl] (2) wt.% eq	[NaCl] wt.%	[LiCl] wt.%	[Na] wt.%	[Li] wt.%	Na/Li ratio
Beauvoir granite (n = 10)															
L1-type	BI-125a	A4	Toz	14	−78	−37.1	275	491	—	36.3	26.5	12.5	10.4	2.0	5.1
L1-type	BI-379a	A6a	Qtz	23	−73	−37.8	~280*	530	34.2	—	26.1	12.9	10.3	2.1	4.9
L1-type	BI-379a	A6b	Qtz	17	−73	−34.8	~280*	527	31.9	—	27.1	11.4	10.7	1.9	5.7
L1-type	BI-379a	A6c	Qtz	19	−69	−35.8	~280*	515	32.6	—	26.6	11.4	10.5	1.9	5.6
L1-type	BI-379a	9a	Qtz	20	−66	−34.0	282	540	—	36.8	28.5	10.5	11.2	1.7	6.5
L1-type	BI-379c	5b	Toz	10	−56	−39.9	~280*	600	36.0	—	24.9	13.1	9.8	2.1	4.6
L1-type	BI-379c	6j	Toz	20	−70	−36.1	~280*	578	32.9	—	26.9	12.1	10.6	2.0	5.3
L2-type	BI-125a	11	Qtz	25	−72	−38.1	404	525	—	47.9	41.6	10.4	16.4	1.7	9.6
L2-type	BI-379a	7a	Qtz	30	−73	−39.9	406	402	—	48.1	41.9	11.1	16.5	1.8	9.0
L2-type	BI-379c	21	Qtz	20	−60	−29.0	354	529	—	42.8	37.8	7.2	14.9	1.2	12.6
La Bosse stockwork (n = 3)															
L1-type	ECH-X2b	44a	Qtz	16	−80	−29.9	~280*	422	28.6	—	30.8	8.2	12.1	1.3	9.0
L1-type	ECH-X2b	44b	Qtz	10	—	−30.0	~280*	377	28.7	—	31.6	8.4	12.4	1.4	9.0
L2-type	ECH-X2b	42	Qtz	15	−81.0	−41.8	~280*	428	37.8	—	25.6	14.4	10.1	2.4	4.3

Salinity in the H_2O-NaCl system was calculated using the ice-melting temperature (1) and the halite dissolution temperature (2); *estimated value; —: not determined.

4.4. LA-ICPMS Analysis of Fluid Inclusions. The different generations of fluid inclusions were analysed by LA-ICPMS, with a focus onto the L1-, L2-, and V2-types, which are interpreted as the earliest fluids exsolved from the Beauvoir granite. The quality of the signals measured by LA-ICPMS depends highly of the size and of the depth of the fluid inclusions in the two ablated minerals (quartz and topaz). A typical LA-ICPMS spectrum of L1-type fluid inclusion from the Beauvoir granite is shown in Figure 11. The fluid inclusion signal is ca. 24 s in length and shows relatively high signal intensities (10^1–10^4 cps) for most of the elements measured (Sn, Cs, Nb, Ta, W, Rb, and Li). The Na signal is low due to the relatively high analytical background (~2,000 cps; LOD ~ 5,300 ppm) of the instrument, which represents a technical limitation for the absolute quantification of the fluid inclusion signals. However, analytical background is generally low (<10 cps) for the other measured elements, excepted for K (~250 cps; LOD ~ 1,700 ppm), Ca (~100 cps; LOD ~ 3,000 ppm), and Mn (~60 cps; LOD ~ 250 ppm). On the 47 fluid inclusions analysed by LA-ICPMS, only 27 yielded interpretable signals and were selected for absolute quantification. The salinity calculated (Table 1) was used to estimate the Na content of the fluid inclusions analysed and used as internal standard for the quantification of the fluid inclusions signals.

Results of LA-ICPMS analysis are given in Table 4 and shown in Figure 12. A discrepancy can be observed between the Na/Li ratios calculated from the microthermometric data and the LA-ICPMS data. Indeed, the Na/Li ratios estimated from microthermometry in the H_2O-NaCl-LiCl system fall in the range 4.3–12.6 (Table 2), whereas those calculated from the LA-ICPMS data are significantly higher and comprised between 0.9 and 33 (Table 4). The latter are not consistent with (i) the very low eutectic temperatures (T_e < −70°C) indicating that the magmatic fluid was Li-rich and (ii) preliminary LIBS analysis on primary L1-type fluid inclusions from the Beauvoir granite, which yielded Na/Li ratios comprised between 1.1 and 2.7 [29]. Therefore, it seems that the Li content is underestimated by LA-ICPMS, thus resulting in higher Na/Li ratios.

4.4.1. Fluid Inclusions in the Beauvoir Granite

L1-Type Fluid Inclusions (n = 5). They are characterized by very high contents in Na (103,500–110,600 ppm), Sn (1,170–38,450 ppm), Cs (22,200–75,650 ppm), K (32,300–41,720 ppm), high contents in Mn (8,930–29,300 ppm), Fe (12,550–16,800 ppm), Rb (1,380–9,330 ppm), Li (4,450–17,960 ppm), and W (920–2,970 ppm) and minor contents in Nb (36–1,450 ppm), Ta (18–180 ppm), and Sr (16–130 ppm). Their Na/Li and Na/K ratios range from 6.2 to 24 and from 2.5 to 4.6, respectively.

V2-Type Fluid Inclusions (n = 2). They have lower concentrations in most of the measured elements compared to the L1-type fluid inclusions and also among all the analysed fluid inclusions in the Beauvoir granite. They are characterized by relatively high contents in Na (71,600–86,200 ppm), Li (25,440–28,480 ppm), K (33,850–46,200 ppm), Cs (19,100–21,600 ppm), Mn (2,640–22,400 ppm), and

Rb (7,360–11,100 ppm) and moderate contents in Sn (1,100–4,270 ppm) and W (250–550 ppm), yielding to ratios Na/Li ~ 3 and Na/K ~ 2.

L2-Type Fluid Inclusions (n = 6). They have among the highest concentrations of the fluid inclusions analysed. They have very high contents in Na (158,200–189,700 ppm), K (65,350–128,000 ppm), Cs (23,700–42,150 ppm), Sn (14,300–75,000 ppm), and Mn (44,550–86,500 ppm), high contents in Li (7,370–51,310 ppm), Fe (22,000–41,800 ppm), and Rb (14,950–44,100 ppm), and relatively high contents in W (1,230–4,250 ppm), Sr (32–84 ppm), Nb (11–1,590 ppm), and Ta (2–2,280 ppm). The Na/Li and Na/K ratios range from 3 to 23 and from 1.5 to 2.6, respectively.

TABLE 3: Salinity estimated from Raman spectrometry data for fluid inclusions analysed using the method of Caumon et al. [45].

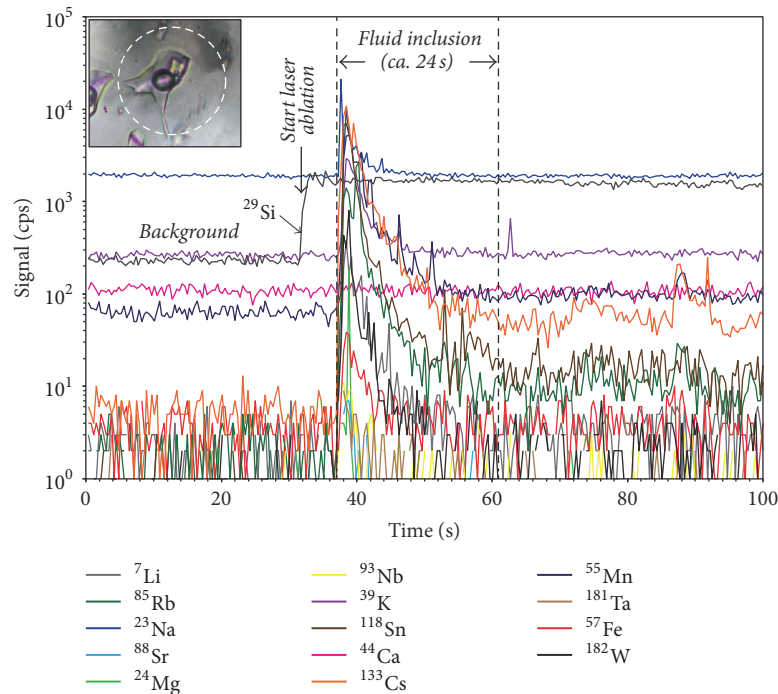| FI-type	Sample	FI n°	Host-mineral	Size μm	[NaCl] wt.% eq
Beauvoir granite (n = 10)					
L1-type	B1-125a	A4	Toz	14	25.7
L1-type	B1-125a	B1	Qtz	16	27.2
L1-type	B1-379a	A6a	Qtz	23	27.0
L1-type	B1-379a	A6b	Qtz	17	26.3
L1-type	B1-379a	A6c	Qtz	19	26.7
L1-type	B1-379c	C1	Qtz	14	28.1
L1-type	B1-379a	9b	Qtz	15	27.8
V2-type	B1-379a	A10a	Qtz	14	18.2
V2-type	B1-379a	A10c	Qtz	18	16.3
V2-type	B1-379a	B4	Qtz	12	4.7
La Bosse stockwork (n = 18)					
L1-type	ECH-X2b	6	Qtz	24	27
V2-type	ECH-X2b	D4	Qtz	42	6.9
V2-type	ECH-11a	D4	Qtz	15	4.1
V2-type	ECH-11a	D2	Qtz	18	2.2
V2-type	ECH-11b	D2	Toz	47	2.1
V2-type	ECH-11b	1a	Qtz	20	1.1
V2-type	ECH-11b	2a	Qtz	45	4.4
L2-type	ECH-X2b	B2	Toz	16	37.6
L3-type	ECH-X2b	A1	Qtz	11	4.4
L3-type	ECH-X2b	A3	Qtz	20	6.0
L3-type	ECH-X2b	A4	Qtz	77	4.5
L3-type	ECH-X2b	B3	Qtz	27	5.9
L3-type	ECH-X2b	C3a	Qtz	35	5.7
L3-type	ECH-X2b	C3b	Qtz	32	5.6
L3-type	ECH-X2c	9a	Toz	10	3.3
L3-type	ECH-X2c	9b	Toz	25	3.5
L3-type	ECH-11b	3a	Qtz	10	2.3
L3-type	ECH-11b	A6	Toz	45	6.6

FIGURE 11: Typical LA-ICPMS spectrum of a primary magmatic L1-type fluid inclusion hosted in a globular quartz crystal from the Beauvoir granite (sample B1-379a; FI n°A6b). The analysed fluid inclusion (picture in inset) is 17 μm in size and was ablated using a laser spot diameter of 32 μm (dashed white circle).

4.4.2. Fluid Inclusions in the La Bosse Stockwork

L1-Type Fluid Inclusions (n = 3). They have very high contents in Na (106,250–112,950 ppm), Fe (58,600–141,800 ppm), Mn (25,300–115,200 ppm), and K (19,350–58,500 ppm), high contents in Cs (9,750–14,800 ppm), and moderate contents in Rb (1,130–1,940 ppm), Li (5,740–9,050 ppm), Sn (580–5,870 ppm), W (185–230 ppm), and Sr (64–200 ppm). Their Na/Li and Na/K ratios range from 12 to 20 and 1.9 to 5.5, respectively.

V2-Type Fluid Inclusions (n = 3). They show the lowest concentrations compared with the L1- and L2-type fluid inclusions in the La Bosse stockwork. Their composition is dominated by high contents in Na (5,500–27,150 ppm), K (10,150–21,360 ppm), and Fe (16,600–49,200 ppm) and moderate contents in Cs (370–5,950 ppm), Sn (60–26,200 ppm), Rb (560–5,230 ppm), Mn (450–25,200 ppm), Mg (1,925–21,250 ppm), Sr (54–630 ppm), W (220–480 ppm), and Li (2,740–5,930 ppm). Their Na/Li and Na/K ratios are comprised between 0.9 and 6.5 and 0.5 and 2.6, respectively.

L2-Type Fluid Inclusions (n = 4). They have very high contents in Na (141,300–144,400 ppm), K (51,500–166,500 ppm), Fe (54,700–232,400 ppm), and Cs (10,900–83,600 ppm), high contents in Sn (2,215–21,600 ppm) and Mn (33,350–98,950 ppm), and moderate contents in Rb (2,410–7,400 ppm), W (240–1,310 ppm), Li (4,260–10,370 ppm), and Sr (91–560 ppm). In some of these fluid inclusions, Nb (63–110 ppm) and Ta (17 ppm) were detected. The Na/Li and Na/K ratios of the L2-type fluid inclusions range from 14 to 33 and from 0.9 to 2.7, respectively.

L3-Type Fluid Inclusions (n = 4). These fluid inclusions were analysed in the quartz and topaz from the metasomatized stockwork. They are characterized by lower contents in Na (13,800–22,050 ppm) and K (3,000–17,700 ppm), relatively high contents in Fe (24,150–170,500 ppm), Mn (21,850–59,550 ppm), Cs (1,150–20,800 ppm), and Sn (200–14,900 ppm), moderate contents in Rb (610–3,340 ppm), Sr (15–4,520 ppm), Li (925–7,610 ppm), and W (920–1,400 ppm), and low contents in Nb (57–160 ppm) and Ta (1.8 ppm). The Na/Li and Na/K ratios are comprised between 2.9 and 19 and 1.2 and 5.9, respectively.

5. Discussion

5.1. Magmatic Signature of the Early Primary Fluids from the Beauvoir Granite. The L1-type fluid inclusions display all the characteristics expected for a primary fluid exsolved from the Beauvoir granite at the magmatic-hydrothermal transition. Microthermometric data show that this is a high-salinity fluid (17–28 wt.% NaCl eq), trapped at high temperature (500 to >600°C), which is also Li-rich (T_e < −70°C) with low Na/Li ~ 5 and low Na/K ≤ 5. These temperatures are close to the solidus temperature of 550–600°C at 1 kbar for the B1 facies of the Beauvoir granite as determined experimentally [57]. The high Na/K (≥1) ratios are typical of magmatic fluids equilibrated with a granitic melt [27, 28, 58], whereas the low Na/Li (≤5) ratios indicate that the fluid was derived from a
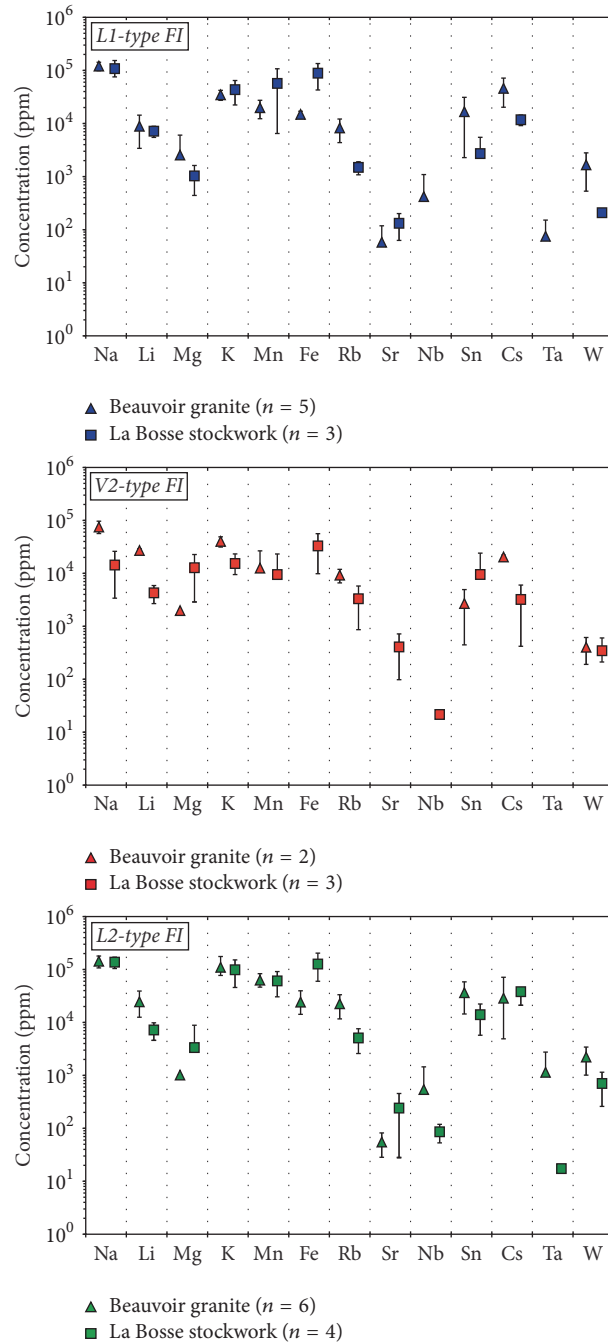
Figure 12: Minor and trace elements contents in L1-, V2- and L2-types fluid inclusions (FI) from the Beauvoir granite and the La Bosse stockwork determined by LA-ICPMS. The values and error bars correspond, respectively, to the averages and standard deviations of the concentrations determined by LA-ICPMS for each fluid inclusion assemblage.

Li-rich magma [59]. Previous preliminary LIBS analysis on L1-type fluid inclusions found in topaz from the Beauvoir granite yielded to lower Na/Li ~ 1–3 [29], which suggest that the very early magmatic fluid may have been even richer in Li. This appears in accordance with the composition of Li-micas in the Beauvoir granite, which represent a late phase on the liquid line of descent of the Beauvoir melt under the low pressure of emplacement estimated [57]. Indeed, these Li-micas display complex internal zoning with compositions ranging from Li-muscovite core to zinnwaldite rim and external lepidolite overgrowth, the latter being interpreted as resulting from the early magmatic-hydrothermal transition [60]. The increase in Li content recorded by the chemical composition of Li-micas appears therefore as a proxy of the progressive exsolution of the early Li-rich magmatic fluid (L1) from the Beauvoir granite.

LA-ICPMS analyses of L1-type fluid inclusions reveal that the chemical composition of this magmatic-hydrothermal

TABLE 4: Chemical compositions of fluid inclusions from the Beauvoir granite and the La Bosse stockwork determined by LA-ICPMS.

FI-type	Sample	FI n°	Host-mineral	Size μm	Salinity wt.% NaCl eq	Na	Li	Mg	K	Ca	Mn	Fe	Rb	Sr	Nb	Sn	Cs	Ta	W	Na/Li	Na/K
Beauvoir granite (*n* = 13)																					
L1-type	BI-379a	9a	Qtz	20	27.0	106250	9140	bdl	23150	bdl	8930	bdl	5000	bdl	180	6250	34550	130	bdl	12	4.6
L1-type	BI-379a	A6a	Qtz	23	27.0	106250	4450	bdl	36560	bdl	21300	12550	9030	16	bdl	18750	22200	18	1110	24	2.9
L1-type	BI-379a	A6b	Qtz	17	26.3	103500	8240	775	41720	bdl	29300	15300	1380	31	41	38450	71700	24	2970	13	2.5
L1-type	BI-379a	A6c	Qtz	19	26.7	105100	4670	bdl	32300	bdl	22800	16800	9330	130	36	18950	75650	22	920	23	3.3
L1-type	BI-379c	C1	Qtz	14	28.1	110600	17960	4770	40000	bdl	17000	bdl	4110	bdl	1450	1170	25900	180	bdl	6.2	2.8
V2-type	BI-379a	10a	Qtz	14	18.2	71600	25440	bdl	33850	bdl	22400	bdl	7360	bdl	bdl	4270	19100	bdl	250	2.8	2.1
V2-type	BI-379c	15v	Qtz	24	21.9	86200	28480	1980	46200	bdl	2640	bdl	1100	bdl	bdl	1100	21600	bdl	550	3.0	1.9
L2-type	BI-379a	7a	Qtz	30	48.1	189300	10900	bdl	82550	bdl	56900	26600	19250	32	17	42500	33600	bdl	1380	17	2.3
L2-type	BI-379c	6l	Toz	15	42.4	166850	7370	bdl	65350	bdl	56900	bdl	14950	bdl	bdl	30150	24100	bdl	2080	23	2.6
L2-type	BI-379c	6m	Toz	25	40.4	159000	11730	1010	72800	bdl	58450	bdl	15600	84	bdl	38850	24550	bdl	2130	14	2.2
L2-type	BI-379c	8a	Qtz	30	44.8	176300	27210	bdl	107150	bdl	85600	41800	20600	49	11	14300	23700	2.2	1230	6.5	1.6
L2-type	BI-379c	8c	Qtz	30	48.2	189700	33600	bdl	128000	bdl	86500	22000	44100	bdl	bdl	17600	24150	bdl	bdl	5.6	1.5
L2-type	BI-379c	9a	Qtz	20	40.2	158200	51310	bdl	82600	bdl	44550	bdl	20600	bdl	1590	75000	42150	2280	4250	3.1	1.9
La Bosse stockwork (*n* = 14)																					
L1-type	ECH-X2b	6	Qtz	24	27.0	106250	9050	615	19350	bdl	115200	141800	1130	64	bdl	580	9750	bdl	230	12	5.5
L1-type	ECH-X2b	44a	Qtz	16	28.6	112550	6740	bdl	52600	bdl	25300	58600	1410	200	bdl	1710	10800	bdl	bdl	17	2.1
L1-type	ECH-X2b	44b	Qtz	10	28.7	112950	5740	1450	58500	bdl	30400	66150	1940	130	bdl	5870	14800	bdl	185	20	1.9
V2-type	ECH-X2b	D4	Qtz	42	6.9	27150	4160	1925	10500	bdl	450	16600	4130	630	22	2200	3300	bdl	220	6.5	2.6
V2-type	ECH-l1b	1a	Qtz	20	1.4	5500	5930	21250	10150	bdl	25200	bdl	560	540	bdl	26200	5950	bdl	480	0.9	0.5
V2-type	ECH-l1b	22a	Qtz	30	2.6	10250	2740	15060	21360	bdl	2730	49200	5230	54	bdl	60	370	bdl	310	3.7	0.5
L2-type	ECH-X2b	B2	Toz	16	36.7	144400	6110	9700	61950	bdl	39500	90900	3500	560	110	16200	10900	17	1310	24	2.3
L2-type	ECH-X2c	21a	Qtz	25	36.3	142850	8060	230	115100	bdl	71800	129000	7400	150	bdl	21600	41700	bdl	670	18	1.2
L2-type	ECH-X2c	22	Qtz	30	35.9	141300	4260	110	51500	bdl	33350	54700	2410	91	bdl	2215	16150	bdl	240	33	2.7
L2-type	ECH-l1a	17a	Qtz	25	36.1	142050	10370	bdl	166500	bdl	98950	232400	7040	165	63	16000	83600	bdl	585	14	0.9
L3-type	ECH-X2c	9b	Toz	25	3.5	13800	3090	4150	6600	bdl	28650	67300	1000	1900	160	8900	20800	bdl	1100	4.5	2.1
L3-type	ECH-X2b	A4	Qtz	77	4.5	17700	925	7810	3000	bdl	21850	24150	610	15.0	57	2870	1150	1.8	920	19	5.9
L3-type	ECH-X2b	C3b	Qtz	32	5.6	22050	7610	26260	17700	bdl	59550	170500	3340	4520	87	14900	10150	bdl	1400	2.9	1.2
L3-type	ECH-l1a	8a	Qtz	16	4.1	16150	1850	bdl	5700	bdl	bdl	bdl	690	bdl	bdl	200	3300	bdl	bdl	8.7	2.8

bdl: below detection limit; Qtz: quartz; Toz: topaz.

fluid is also rich (10^2–10^4 ppm) in Rb and Cs and in rare-metals (W, Nb, Ta, and Li). The very high and highly variable concentration of Sn in the L1 fluid (up to 4 wt.% Sn) may be however questioned. Considering that only one microcrystal of cassiterite was found in one L1-type fluid inclusion, as identified by Raman spectrometry, it may be suspected that the high Sn contents in the L1 fluid reflect the heterogeneous trapping of nanoinclusions of cassiterite rather than oversaturation of the magmatic fluid relatively to SnO$_2$. Another possible explanation would be the formation of cassiterite daughter crystals directly from the trapped magmatic fluid, which can reach very high concentrations (>1 wt.%) for some metals under supercritical condition [61]. The Nb content (36–1,450 ppm) is higher on average than the Ta content (18–180 ppm) in the L1 fluid, with an average Nb/Ta ratio ~ 5.6. This appears contradictory by comparison with the composition of the B1 facies from the Beauvoir granite, which has higher Ta than Nb contents, with Nb/Ta ratio in the range of 0.4–0.9 and ~0.6 on average [12, 13]. Similarly Ta > Nb contents were also found in other PHP-RMG worldwide, for instance, in Portugal (Argemela granite [62]), France (Montebras granite [13]), Germany (Ehrenfriedersdorf pegmatite [63]), and China (Yichun granite [13]; Laohutou granite [64]). Due to the higher solubility of tantalite relative to that of columbite in peraluminous granitic magmas [3, 65], one can expect a late Ta enrichment relative to Nb in the residual melt and thus a high Ta/Nb ratio in the exsolved magmatic fluid, despite low partition coefficients for Nb and Ta between an aqueous fluid and silicate melt in granitic systems ($D^{\text{fluid-melt}}$ [Ta] < $D^{\text{fluid-melt}}$ [Nb] < 0.1) [3, 66–68]. Nevertheless, several works on RMG have demonstrated the existence of a late subsolidus fluid-rock interaction between the primary magmatic-hydrothermal fluid and the rare-metal minerals (mainly columbite-tantalite) hosted in the granitic melt, leading to a late Ta enrichment as veinlets and overgrowths of tantalite, wodginite, Ta-rich rutile, or Ta-rich cassiterite on early-formed columbite of magmatic origin, following a two-stage evolution and separated in time by a resorption-corrosion event (e.g., [69–72]). These late mineral associations are interpreted as markers of the magmatic-hydrothermal transition in RMG, thus yielding to relative Ta depletion and Nb enrichment in the exsolved magmatic-hydrothermal fluid. In the B1 facies from the Beauvoir granite, replacement of early magmatic columbite by late microlite was also evidenced and was interpreted as the interaction of the late magmatic fluid with the early Nb-Ta oxides [73]. This may therefore suggest the higher mobility of Nb compared to Ta in the magmatic-hydrothermal fluid derived from the Beauvoir granite, in accordance with the Nb > Ta contents determined in the L1-type fluid inclusions, despite a low Nb/Ta ratio initially in the Beauvoir granite.

Comparing the composition of the L1-type fluid inclusions contained in the primary quartz and topaz from the Beauvoir granite with the whole-rock composition of the B1 facies (Figure 13), it appears that the primary L1 fluid is more enriched on average for most of the measured elements (W, Nb, Mg, Fe, Mn, Cs, Sn, Rb, and Na). Ta and K have similar concentrations in the B1 granite and in the L1 fluid, suggesting
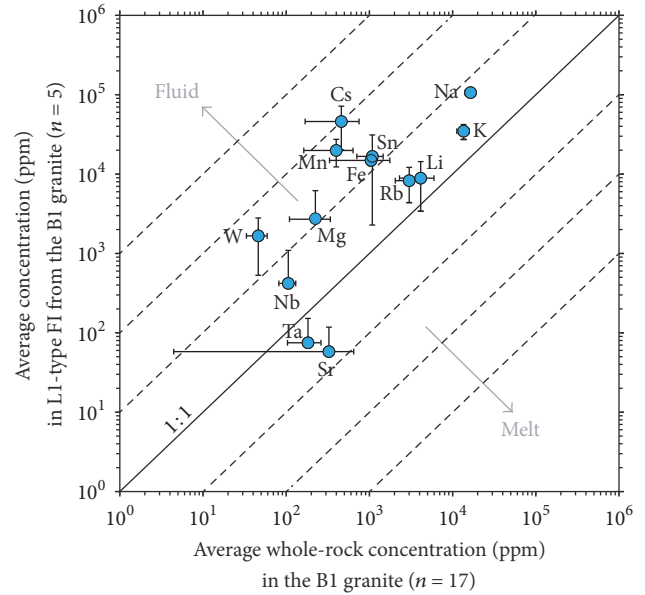

FIGURE 13: Average concentration of L1-type fluid inclusions (FI) contained in primary quartz from the Beauvoir B1 granite determined by LA-ICPMS ($n = 5$) versus average whole-rock concentration of the B1 granite ($n = 17$) compiled from Cuney et al. [12] and Raimbault et al. [13].

no significant fluid/melt partitioning. Ca was systematically below the limits of detection (LOD ~ 3,000 ppm) in the L1-type fluid inclusions, while Sr is at low concentrations (10–100 ppm). This is in contrast with the relatively high contents in the B1 facies from the Beauvoir granite in both Ca (5,000 ppm on average and up to 11,500 ppm [12, 13]) and Sr (325 ppm on average and up to 1,240 ppm [12, 13]). This discrepancy likely reflects a Ca and Sr input from the surroundings micaschists by external fluids, as evidenced for Sr by the presence of secondary low-temperature minerals of Sr-rich phosphates in the Beauvoir granite [74]. Thus, these results indicate that most of the elements partition preferentially into the magmatic fluid rather than into the crystallizing melt.

F and Cl were not measured by LA-ICPMS since they have high first ionization potentials, yielding to elevated LOD due to low sensitivity. However, there are several evidences that the primary magmatic fluids from the Beauvoir granite were Cl-rich, as indicated by (i) the high salinity (up to 28.1 wt.% NaCl eq) calculated for the L1-type fluid inclusions and (ii) the high Sn content in the fluid inclusions, although likely overestimated, which suggests that Sn was transported as Sn-Cl complexes in the fluid [75, 76]. Concerning F, there are also indications for an elevated content of F in the magmatic fluid. Firstly, despite the low fluid-melt partition coefficient of F ($D^{\text{fluid-melt}}$ [F] = 0.4 at 650°C and 2 kbar [77]), the very high F content in the B1 granite (2.3 wt.% on average [12, 13]) implies a high F concentration in the exsolved fluid. As pointed by Cuney et al. [12], owing to the large F halo around the B1 granitic cupola, which was evidently provided by the exsolved fluid, the initial F content in the Beauvoir

B1 melt would have been in the order of 4 wt.%. This has been confirmed by in situ electron microprobe analysis of melt inclusions from the B1 facies, which yielded to average F content of 4.9 wt.% [78]. A similar F content of 4 wt.% was also measured, for instance, in primary melt inclusions from the Zinnwald RMG [22]. Thus, considering an initial F content of 4-5 wt.% in the initial Beauvoir granitic melt and using a fluid-melt partition coefficient of 0.4 [77], an approximate content of 1.6–2.0 wt.% F in the exsolved magmatic fluid may be estimated. Secondly, the crystallization of massive topazite and the partial dissolution of the quartz veins in the La Bosse stockwork imply that the magmatic fluid was F- and Al-rich and undersaturated relatively to SiO_2 and has slightly interacted with the enclosing rocks. Finally, the relatively high contents of Nb and Ta in the L1 fluid are also consistent with a high concentration of F, which has been shown to increase significantly the solubility of Nb and Ta in hydrothermal solutions [79, 80]. This resulted in the precipitation of Nb (and Ta) as columbite-tantalite and wolframoixiolite in microvugs during the topazification of the quartz-ferberite stockwork [42].

5.2. Chemical Evolution of the Magmatic Fluids Exsolved from the Beauvoir Granite.

The Beauvoir granite constitutes a remarkable example of a PHP-RMG that crosscuts an early quartz-ferberite stockwork with a vertical development of more than 100 m. The studied quartz-topaz vein from the La Bosse stockwork is located at about 100 m above and several 100 m laterally from the roof of the granitic cupola (Figure 2). This implies that when the magmatic-hydrothermal fluids exsolved from the B1 granite reached the stockwork, they had circulated through the surrounding micaschists along a distance of several 100 m and had therefore likely interacted with them. A comparison between the primary fluids (L1, L2, and V2) found within the granite and those in the stockwork should therefore allow characterizing this interaction. At the first order, the different types of fluids encountered in the stockwork are similar to those from the Beauvoir granite. However, at the second order, microthermometric data show a decreasing trend of T_H and salinity in fluid inclusions from the Beauvoir granite to the La Bosse stockwork (Figure 9). The T_H decrease is of 60 to 120°C on average from the granite to the stockwork, which may be interpreted in terms of cooling and thermal equilibration around the granitic intrusion. The salinity decrease is of 3 to 10 wt.% NaCl eq on average, which suggests that the magmatic-hydrothermal fluids were variably diluted by an external low-salinity fluid. A possibility for such fluid may be meteoric water, considering the relatively shallow depth of emplacement (~3 km) of the Beauvoir granite estimated from fluid inclusion studies [46]. By contrast, there is no direct evidence for interaction of the primary magmatic fluids with metamorphic fluids. The latter were only identified in early fluid inclusions disseminated within the deformed quartz (Q1) of the La Bosse vein system and were interpreted as related to the formation of the W stockwork [46], which precede the emplacement of the Beauvoir granite from ca. 20 Ma [40].

The chemical composition of the L1 fluid exhibits small, but significant, differences between the Beauvoir granite and the La Bosse stockwork (Figure 12). On the one hand, the elements Mg, Rb, Cs, Nb, Ta, Sn, and W decrease; on the other hand Mn, Fe, and Sr increase progressively, from the granite to the stockwork. These variations may be interpreted either as recording fluid-rock interactions of the magmatic fluids with the surrounding micaschists, or as direct interactions with the quartz-ferberite stockwork. Similar chemical trends are observed for the L2 and V2 fluids, excepted for Mg and W that show higher concentrations in fluid inclusions from the La Bosse stockwork compared to the Beauvoir granite. The W enrichment in some V2 fluid inclusions may come from interaction with the ferberite of the stockwork, whereas the lack of Nb and Ta in L2 fluid inclusions may be the result of their trapping in the wolframoixiolite and columbo-tantalite, which crystallized in microvugs within the partially dissolved ferberite. The variations in concentrations observed for the other elements, however, may be due to a direct fluid-rock interaction with the micaschists marked by a gain of Mn, Fe, and Sr into the fluid, and by a loss of Mg, Rb, Cs, Nb, Ta, Li, and Sn into the host-rocks. In this regard, the introduction of Sr leached from the micaschists by external fluids into the Beauvoir granite was demonstrated by Charoy et al. [74].

Finally, it remains remarkable that the geochemical signature of the RMG is still preserved in the primary L1-type fluid inclusions from the metasomatized La Bosse stockwork, despite the distance from the granitic cupola (>100 m) and interaction with the host-rocks and external fluids. Furthermore, the undersaturation relatively to SiO_2 of the fluid suggests an overall rapid transfer from the granitic cupola through the surrounding rocks, likely using the quartz-ferberite vein system as preferential flow channel. Consequently, it may be tentatively proposed that the geochemical signature of fluid inclusions represents a proximal pathfinder for the discovery of hidden rare-metal granitic cupolas in the surroundings of the Echassières granitic complex and more widely in the Limousin area, as well as elsewhere in the world.

5.3. Element Partitioning between Coexisting Vapour and Brine during Early Boiling.

Determining the major and trace elements composition of coexisting V2- and L2-type fluid inclusions that formed during the early boiling of the primary L1 fluid at ca. 400–520°C allows studying the element partitioning between the low-density vapour (V2) and the high-density brine (L2). Vapour-brine distribution coefficients determined by LA-ICPMS analysis for the coexisting V2- and L2-type fluid inclusions in the Beauvoir granite and in the La Bosse stockwork are shown in Figure 14. In the Beauvoir granite, the majority of the elements (Na, K, Mn, Rb, Sn, Cs, and W) partitions preferentially into the brine, whereas only Mg and Li are preferentially enriched into the vapour. In the La Bosse stockwork, the trend is almost similar with the only difference that Li and Sr are more enriched into the brine. These results are in good agreement with those of Audétat et al. [28] for the Mole granite, thus confirming that most of the elements display a preferential partitioning for the Cl-rich aqueous phase.
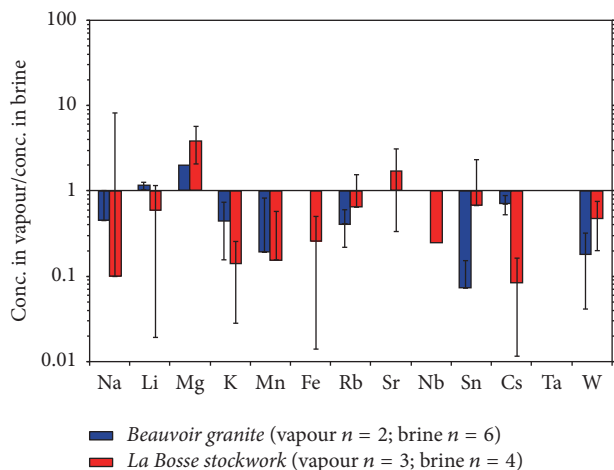
FIGURE 14: Vapour-brine distribution coefficients determined by LA-ICPMS analysis of coexisting V2- and L2-type fluid inclusions from the Beauvoir granite and the La Bosse stockwork. Columns represent the average value calculated for each fluid inclusion population, whereas error bars indicate the standard deviation (1σ) associated with these averages.

6. Conclusions

This work allowed characterizing the geochemical signature of the magmatic-hydrothermal fluids exsolved from the Beauvoir rare-metal granite. The different generations of fluid inclusions (L1, L2, V2, and L3) initially identified by Aïssa et al. [46] were retrieved during this study. The L1-type fluid inclusions represent the earliest records of the primary magmatic fluid in the Beauvoir granite. Microthermometric data showed that this fluid is of high temperature (500 to >600°C) and high salinity (17–28 wt.% NaCl eq) and is Li-rich ($T_e < -70$°C) with Na/Li ratios ~ 5. LA-ICPMS analyses show that the chemical composition of the L1 fluid is dominated by Na, K, Cs, and Rb, with significant concentrations (10^1–10^4 ppm) in rare-metals (W, Nb, Ta, Sn, and Li). Boiling of the L1 fluid at ca. 450°C yielded by phase separation to a low- to moderate-salinity vapour (V2; 4.7–22 wt.% NaCl eq) and a high-salinity brine (L2; 32–48 wt.% NaCl eq). LA-ICPMS analyses of these two types of fluid inclusions revealed that the L2-type fluid inclusions have the highest concentrations in metals and show a preferential enrichment in most of the elements (Na, K, Mn, Fe, Rb, Nb, Sn, Cs, and W) compared to the V2-type fluid inclusions. The evolution of the exsolved magmatic fluids with distance from the Beauvoir granitic cupola is characterized by a systematic decrease in temperature and salinity. The temperature decrease can be interpreted in terms of cooling and thermal equilibration around the intrusion, whereas the salinity decrease indicates that the exsolved magmatic-hydrothermal fluids were more or less diluted by a low-salinity fluid, possibly of meteoric origin. These results demonstrate that primary fluid inclusions preserved the pristine signature of the magmatic-hydrothermal fluids in the Beauvoir granite, but also in the metasomatized W stockwork, despite the distance from the granitic cupola (>100 m) and interaction with external fluids.

Consequently, it is proposed that the geochemical signature of fluid inclusions may serve as a possible pathfinder for the discovery of hidden rare-metal granitic cupolas at Echassières and more widely in the Limousin area, as elsewhere in the world.

Disclosure

Conflicts of Interest

The authors declare that they have no conflicts of interest.

Acknowledgments

References

[1] P. J. Pollard, "A special issue devoted to the geology of rare metal deposits; geology of rare metal deposits; an introduction and overview," *Economic Geology*, vol. 90, no. 3, pp. 489–494, 1995.

[2] R. L. Linnen, M. Van Lichtervelde, and P. Černý, "Granitic pegmatites as sources of strategic metals," *Elements*, vol. 8, no. 4, pp. 275–280, 2012.

[3] R. L. Linnen and M. Cuney, "Granite-related rare-element deposits and experimental constraints on Ta-Nb-W-Sn-Zr-Hf mineralization," in *Rare-Element Geochemistry and Mineral Deposits Short Course Notes*, R. L. Linnen and I. M. Samson, Eds., vol. 17, pp. 45–68, Geological Association of Canada, Canada, 2005.

[4] P. Černý and T. S. Ercit, "The classification of granitic pegmatites revisited," *The Canadian Mineralogist*, vol. 43, no. 6, pp. 2005–2026, 2005.

[5] P. Černý, P. L. Blevin, M. Cuney, and D. London, "Granite-Related Ore Deposits," *Economic Geology 100 th anniversary volume*, vol. 107, no. 2, pp. 383-384, 2005.

[6] Y. Chen, A. H. Clark, E. Farrar, H. A. H. P. Wasteneys, M. J. Hodgson, and A. V. Bromley, "Diachronous and independent histories of plutonism and mineralization in the Cornubian Batholith, southwest England," *Journal of the Geological Society*, vol. 150, no. 6, pp. 1183–1191, 1993.
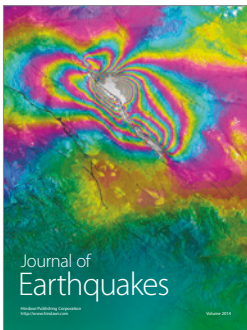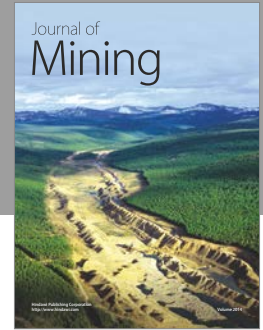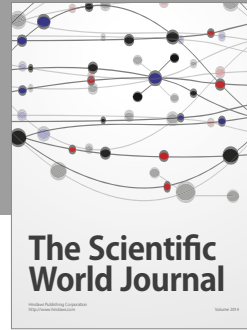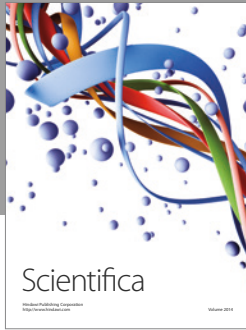
[7] C. Marignac and M. Cuney, "Ore deposits of the French Massif Central: Insight into the metallogenesis of the Variscan collision belt," *Mineralium Deposita*, vol. 34, no. 5-6, pp. 472–504, 1999.

[8] M. Cuney, P. Alexandrov, C. L. C. De Veslud et al., "The timing of W-Sn-rare metals mineral deposit formation in the Western Variscan chain in their orogenic setting: The case of the Limousin area (Massif Central, France)," *Geological Society of London, Special Publication*, vol. 204, pp. 213–228, 2002.

[9] J. Melleton, E. Gloaguen, D. Frei, M. Novák, and K. Breiter, "How are the emplacement of rare-element pegmatites, regional metamorphism and magmatism interrelated in the Moldanubian domain of the Variscan Bohemian Massif, Czech Republic?" *The Canadian Mineralogist*, vol. 50, no. 6, pp. 1751–1773, 2012.

[10] J. Melleton, E. Gloaguen, and D. Frei, "Rare-elements (Li-Be-Ta-Sn-Nb) magmatism in the European Variscan Belt, a review," in *Proceedings of the 13th Biennial SGA Meeting*, A. S. André-Mayer, M. Cathelineau, P. Muchez, E. Pirard, and S. Sindern, Eds., vol. 2, pp. 24–27, France, 2015.

[11] M. Cuney and A. Autran, "Objectifs généraux du projet GPF Echassières n°1 et résultats essentiels acquis par le forage de 900 m sur le granite albitique à topaze-lépidolite de Beauvoir," in *Géologie profonde de la France, Echassières : le forage scientifique. Une clé pour la compréhension des mécanismes magmatiques et hydrothermaux associés aux granites à métaux rares*, M. Cuney and A. Autran, Eds., pp. 7–24, Géologie de la France, 1987.

[12] M. Cuney, C. Marignac, and A. Weisbrod, "The Beauvoir topaz-lepidolite albite granite (Massif Central, France) : the disseminated magmatic Sn-Li-Ta-Nb-Be mineralization," *Economic Geology*, vol. 87, no. 7, pp. 1766–1794, 1992.

[13] L. Raimbault, M. Cuney, C. Azencott, J. L. Duthou, and J. L. Joron, "Geochemical evidence for a multistage magmatic genesis of Ta-Sn-Li mineralization in the granite at Beauvoir, French Massif Central," *Economic Geology*, vol. 90, no. 3, pp. 548–576, 1995.

[14] K. Breiter, A. Müller, J. Leichmann, and A. Gabašová, "Textural and chemical evolution of a fractionated granitic system: The Podlesí stock, Czech Republic," *Lithos*, vol. 80, no. 1-4, pp. 323–345, 2005.

[15] Z. Johan and V. Johan, "Accessory minerals of the Cínovec (Zinnwald) granite cupola, Czech Republic: Indicators of petrogenetic evolution," *Mineralogy and Petrology*, vol. 83, no. 1-2, pp. 113–150, 2005.

[16] J. D. Webster, J. R. Holloway, and R. L. Hervig, "Partitioning of lithophile trace elements between H_2O and $H_2O + CO_2$ fluids and topaz rhyolite melt," *Economic Geology*, vol. 84, no. 1, pp. 116–134, 1989.

[17] R. L. Linnen, "The solubility of Nb-Ta-Zr-Hf-W in granitic melts with Li and Li + F: Constraints for mineralization in rare metal granites and pegmatites," *Economic Geology*, vol. 93, no. 7, pp. 1013–1025, 1998.

[18] I. V. Veksler, "Liquid immiscibility and its role at the magmatic-hydrothermal transition: a summary of experimental studies," *Chemical Geology*, vol. 210, no. 1-4, pp. 7–31, 2004.

[19] I. V. Veksler, "Element enrichment and fractionation by magmatic aqueous fluids: experimental constraints on melt-fluid immiscibility and element partitioning," in *Rare-Element Geochemistry and Mineral Deposits Short Course Notes*, R. L. Linnen and I. M. Samson, Eds., vol. 17, pp. 69–85, Geological Association of Canada, Canada, 2005.

[20] R. Thomas, H.-J. Förster, and W. Heinrich, "The behaviour of boron in a peraluminous granite-pegmatite system and associated hydrothermal solutions: a melt and fluid-inclusion study," *Contributions to Mineralogy and Petrology*, vol. 144, no. 4, pp. 457–472, 2003.

[21] R. Thomas, H.-J. Förster, K. Rickers, and J. D. Webster, "Formation of extremely F-rich hydrous melt fractions and hydrothermal fluids during differentiation of highly evolved tin-granite magmas: a melt/fluid-inclusion study," *Contributions to Mineralogy and Petrology*, vol. 148, no. 5, pp. 582–601, 2005.

[22] J. Webster, R. Thomas, H.-J. Förster, R. Seltmann, and C. Tappen, "Geochemical evolution of halogen-enriched granite magmas and mineralizing fluids of the Zinnwald tin-tungsten mining district, Erzgebirge, Germany," *Mineralium Deposita*, vol. 39, no. 4, pp. 452–472, 2004.

[23] E. V. Badanina, I. V. Veksler, R. Thomas, L. F. Syritso, and R. B. Trumbull, "Magmatic evolution of Li-F, rare-metal granites: a case study of melt inclusions in the Khangilay complex, Eastern Transbaikalia (Russia)," *Chemical Geology*, vol. 210, no. 1-4, pp. 113–133, 2004.

[24] K. Rickers, R. Thomas, and W. Heinrich, "Trace-element analysis of individual synthetic and natural fluid inclusions with synchrotron radiation XRF using Monte Carlo simulations for quantification," *European Journal of Mineralogy*, vol. 16, no. 1, pp. 23–35, 2004.

[25] K. Rickers, R. Thomas, and W. Heinrich, "The behavior of trace elements during the chemical evolution of the H_2O-, B-, and F-rich granite-pegmatite-hydrothermal system at Ehrenfriedersdorf, Germany: a SXRF study of melt and fluid inclusions," *Mineralium Deposita*, vol. 41, no. 3, pp. 229–245, 2006.

[26] A. Y. Borisova, R. Thomas, S. Salvi, F. Candaudap, A. Lanzanova, and J. Chmeleff, "Tin and associated metal and metalloid geochemistry by femtosecond LA-ICP-QMS microanalysis of pegmatite-leucogranite melt and fluid inclusions: New evidence for melt-melt-fluid immiscibility," *Mineralogical Magazine*, vol. 76, no. 1, pp. 91–113, 2012.

[27] A. Audétat, D. Günther, and C. A. Heinrich, "Magmatic-hydrothermal evolution in a fractionating granite: A microchemical study of the Sn-W-F-mineralized mole granite (Australia)," *Geochimica et Cosmochimica Acta*, vol. 64, no. 19, pp. 3373–3393, 2000.

[28] A. Audétat, D. Güther, and C. A. Heinrich, "Causes for Large-Scale Metal Zonation around Mineralized Plutons: Fluid Inclusion LA-ICP-MS Evidence from the Mole Granite, Australia," *Economic Geology*, vol. 95, no. 8, pp. 1563–1581, 2000.

[29] C. Fabre, MC. Boiron, C. Marignac, and M. Aïssa, "Li-F-rich magmatic fluids exsolved from rare metal granites: the example of the Beauvoir granite (French Massif Central); a microthermometric and LIBS study. XVI ECROFI abstract," *Porto*, vol. 7, pp. 145–147, 2001.

[30] M. Faure, J.-M. Lardeaux, and P. Ledru, "A review of the pre-Permian geology of the Variscan French Massif Central," *Comptes Rendus — Geoscience*, vol. 341, no. 2-3, pp. 202–213, 2009.

[31] J. L. Duthou, J. M. Cantagrel, J. Didier, and Y. Vialette, "Palaeozoic granitoids from the French Massif Central: age and origin studied by [87]Rb-[87]Sr system," *Physics of the Earth and Planetary Interiors*, vol. 35, no. 1-3, pp. 131–144, 1984.

[32] C. Cartannaz, P. Rolin, A. Cocherie et al., "Characterization of wrench tectonics from dating of syn- to post-magmatism in the north-western French Massif Central," *International Journal of Earth Sciences*, vol. 96, no. 2, pp. 271–287, 2007.

[33] C. Pin, "Sr-Nd isotopic study of igneous and metasedimentary enclaves in some Hercynian granitoids from the Massif Central," in *Enclaves and granite petrology*, J. Didier and B. Barbarin, Eds., vol. 13, pp. 333–343, Elsevier, France, 1991.

[34] M. Faure, J. Grolier, and J. Pons, "Extensional ductile tectonics of the Sioule metamorphic series (Variscan French Massif Central)," *Geologische Rundschau*, vol. 82, no. 3, pp. 461–474, 1993.

[35] B. Schulz, "EMP-monazite age controls on P-T paths of garnet metapelites in the Variscan inverted metamorphic sequence of la Sioule, French Massif Central," *Bulletin de la Société Géographique de France*, vol. 180, no. 3, pp. 271–282, 2009.

[36] D. Do Couto, M. Faure, R. Augier et al., "Monazite U–Th–Pb EPMA and zircon U–Pb SIMS chronological constraints on the tectonic, metamorphic, and thermal events in the inner part of the Variscan orogen, example from the Sioule series, French Massif Central," *International Journal of Earth Sciences*, vol. 105, no. 2, pp. 557–579, 2016.

[37] J. L. Vigneresse, "Organisation tridimensionnelle du massif d'Echassières et bilan des mesures géophysiques de surface," in *In Géologie profonde de la France, Echassières : le forage scientifique. Une clé pour la compréhension des mécanismes magmatiques et hydrothermaux associés aux granites à métaux rares*, M. Cuney and A. Autran, Eds., pp. 27–32, Géologie de la France, France, 1987.

[38] A. Cheilletz, D. Archibald, M. Cuney, and B. Charoy, "Ages ^{40}Ar/^{39}Ar du leucogranite à topaze-lépidolite de Beauvoir et des pegmatites sodolithiques de Chédeville (Nord Massif Central, France)," *Significations pétrologique et géodynamique. Comptes Rendus de l'Académie des Sciences*, vol. 315, pp. 329–336, 1992.

[39] T. Merceron, P. Vieillard, A.-M. Fouillac, and A. Meunier, "Hydrothermal alterations in the Echassières granitic cupola (Massif central, france)," *Contributions to Mineralogy and Petrology*, vol. 112, no. 2-3, pp. 279–292, 1992.

[40] M. Harlaux, R. L. Romer, J. Mercadier, C. Morlot, C. Marignac, and M. Cuney, "40 Ma of hydrothermal W mineralization during the Variscan orogenic evolution of the French Massif Central revealed by U-Pb dating of wolframite," *Mineralium Deposita*, pp. 1–31, 2017.

[41] G. Aubert, "Les coupoles granitiques de Montebras et d'Echassières (Massif Central Français) et la genèse de leurs minéralisations en étain, lithium, tungstène et béryllium," *Mémoires du BRGM*, vol. 46, p. 350, 1969.

[42] M. Aïssa, C. Marignac, and A. Weisbrod, "Le stockwerk à ferbérite d'Echassières : évolution spatiale et temporelle ; cristallochimie des ferbérites," in *Géologie profonde de la France, d'Echassières : le forage scientifique. Une clé pour la compréhension des mécanismes magmatiques et hydrothermaux associés aux granites à métaux rares*, M. Cuney and A. Autran, Eds., pp. 311–333, Géologie de la France, France, 1987.

[43] R. J. Bodnar, "Introduction to aqueous-electrolyte fluid inclusions. Mineralogical Association of Canada," *Short Course*, vol. 32, pp. 81–99, 2003.

[44] D. Michel, M. Christophe, C. Teddy et al., "Investigation of the H_2O-NaCl-LiCl system: A synthetic fluid inclusion study and thermodynamic modeling from -50◦ to +100◦C and up to 12 mol/kg," *Economic Geology*, vol. 105, no. 2, pp. 329–338, 2010.

[45] M.-C. Caumon, J. Dubessy, P. Robert, and A. Tarantola, "Fused-silica capillary capsules (FSCCs) as reference synthetic aqueous fluid inclusions to determine chlorinity by Raman spectroscopy," *European Journal of Mineralogy*, vol. 25, no. 5, pp. 755–763, 2013.

[46] M. Aïssa, A. Weisbrod, and C. Marignac, "Caractéristiques chimiques et thermodynamiques des circulations hydrothermales du site d'Echassières," in *Géologie profonde de la France, Echassières : le forage scientifique. Une clé pour la compréhension des mécanismes magmatiques et hydrothermaux associés aux granites à métaux rares*, M. Cuney and A. Autran, Eds., pp. 335–350, Géologie de la France, 1987.

[47] E. Roedder, "The origin of inclusions.," *Reviews in Mineralogy, Volume 12: Fluid Inclusions, (Mineralogical Society of America)*, pp. 11–45, 1984.

[48] E. Roedder, "Fluid inclusion analysis-Prologue and epilogue," *Geochimica et Cosmochimica Acta*, vol. 54, no. 3, pp. 495–507, 1990.

[49] L. W. Diamond, "Review of the systematics of CO_2-H_2O fluid inclusions," *Lithos*, vol. 55, no. 1-4, pp. 69–99, 2001.

[50] D. Günther, A. Audétat, R. Frischknecht, and C. A. Heinrich, "Quantitative analysis of major, minor and trace elements in fluid inclusions using laser ablation-inductively coupled plasma mass spectrometry," *Journal of Analytical Atomic Spectrometry*, vol. 13, no. 4, pp. 263–270, 1998.

[51] K. P. Jochum, U. Weis, B. Stoll et al., "Determination of reference values for NIST SRM 610-617 glasses following ISO guidelines," *Geostandards and Geoanalytical Research*, vol. 35, no. 4, pp. 397–429, 2011.

[52] M. B. Fricker, *Design of ablation cells for LA-ICP-MS : from modeling to high spatial resolution analysis applications. [Ph. D. Thesis]*, 2012.

[53] M. M. Allan, B. W. D. Yardley, L. J. Forbes, K. I. Shmulovich, D. A. Banks, and T. J. Shepherd, "Validation of LA-ICP-MS fluid inclusion analysis with synthetic fluid inclusions," *American Mineralogist*, vol. 90, no. 11-12, pp. 1767–1775, 2005.

[54] H. P. Longerich, S. E. Jackson, and D. Günther, "Laser ablation inductively coupled plasma mass spectrometric transient signal data acquisition and analyte concentration calculation," *Journal of Analytical Atomic Spectrometry*, vol. 11, no. 9, pp. 899–904, 1996.

[55] C. Monnin, M. Dubois, N. Papaiconomou, and J.-P. Simonin, "Thermodynamics of the LiCl + H_2O system," *Journal of Chemical & Engineering Data*, vol. 47, no. 6, pp. 1331–1336, 2002.

[56] J. Dubessy, T. Lhomme, M.-C. Boiron, and F. Rull, "Determination of chlorinity in aqueous fluids using Raman spectroscopy of the stretching band of water at room temperature: Application to fluid inclusions," *Applied Spectroscopy*, vol. 56, no. 1, pp. 99–106, 2002.

[57] M. Pichavant, M. Boher, J. F. Stenger, M. Aïssa, and B. Charoy, "Relations de phase des granites de Beauvoir à 1 et 3 kbar, en condition de saturation en H_2O," in *Géologie profonde de la France, Echassières : le forage scientifique. Une clé pour la compréhension des mécanismes magmatiques et hydrothermaux associés aux granites à métaux rares*, M. Cuney and A. Autran, Eds., pp. 77–85, Géologie de la France, France, 1987.

[58] A. H. Rankin, M. H. Ramsey, B. Coles, F. Van Langevelde, and C. R. Thomas, "The composition of hypersaline, iron-rich granitic fluids based on laser-ICP and Synchrotron-XRF microprobe analysis of individual fluid inclusions in topaz, Mole granite, eastern Australia," *Geochimica et Cosmochimica Acta*, vol. 56, no. 1, pp. 67–79, 1992.

[59] M. Cathelineau, C. Marignac, M.-C. Boiron, G. Gianelli, and M. Puxeddu, "Evidence for Li-rich brines and early magmatic fluid-rock interactionin the Larderello geothermal system," *Geochimica et Cosmochimica Acta*, vol. 58, no. 3, pp. 1083–1099, 1994.

[60] G. Monier, B. Charoy, M. Cuney, D. Ohnenstetter, and J. L. Robert, "Evolution spatiale et temporelle de la composition des micas du granite albitique à topaze-lépidolite de Beauvoir," in *In Géologie profonde de la France, Echassières : le forage scientifique. Une clé pour la compréhension des mécanismes magmatiques et hydrothermaux associés aux granites à métaux rares*, M. Cuney and A. Autran, Eds., pp. 179–188, Géologie de la France, France, 1987.

[61] R. Thomas and P. Davidson, "Revisiting complete miscibility between silicate melts and hydrous fluids, and the extreme enrichment of some elements in the supercritical state - Consequences for the formation of pegmatites and ore deposits," *Ore Geology Reviews*, vol. 72, pp. 1088–1101, 2016.

[62] B. Charoy and F. Noronha, "Multistage growth of a rare-element, volatile-rich microgranite at argemela (Portugal)," *Journal of Petrology*, vol. 37, no. 1, pp. 73–94, 1996.

[63] J. D. Webster, R. Thomas, D. Rhede, H.-J. Förster, and R. Seltmann, "Melt inclusions in quartz from an evolved peraluminous pegmatite: Geochemical evidence for strong tin enrichment in fluorine-rich and phosphorus-rich residual liquids," *Geochimica et Cosmochimica Acta*, vol. 61, no. 13, pp. 2589–2604, 1997.

[64] J.-C. Zhu, R.-K. Li, F.-C. Li, X.-L. Xiong, F.-Y. Zhou, and X.-L. Huang, "Topaz-albite granites and rare-metal mineralization in the Limu district, Guangxi Province, Southeast China," *Mineralium Deposita*, vol. 36, no. 5, pp. 393–405, 2001.

[65] R. L. Linnen and H. Keppler, "Columbite solubility in granitic melts: Consequences for the enrichment and fractionation of Nb and Ta in the Earth's crust," *Contributions to Mineralogy and Petrology*, vol. 128, no. 2-3, pp. 213–227, 1997.

[66] H. Keppler, "Constraints from partitioning experiments on the composition of subduction-zone fluids," *Nature*, vol. 380, no. 6571, pp. 237–240, 1996.

[67] V. Y. Chevychelov, G. P. Zaraisky, S. E. Borisovskii, and D. A. Borkov, "Effect of melt composition and temperature on the partitioning of Ta, Nb, Mn, and F between granitic (alkaline) melt and fluorine-bearing aqueous fluid: Fractionation of Ta and Nb and conditions of ore formation in rare-metal granites," *Petrology*, vol. 13, no. 4, pp. 305–321, 2005.

[68] G. P. Borodulin, V. Y. Chevychelov, and G. P. Zaraysky, "Experimental study of partitioning of tantalum, niobium, manganese, and fluorine between aqueous fluoride fluid and granitic and alkaline melts," *Doklady Earth Sciences*, vol. 427, no. 1, pp. 868–873, 2009.

[69] K. Breiter, R. Škoda, and P. Uher, "Nb-Ta-Ti-W-Sn-oxide minerals as indicators of a peraluminous P- and F-rich granitic system evolution: Podlesí, Czech Republic," *Mineralogy and Petrology*, vol. 91, no. 3-4, pp. 225–248, 2007.

[70] L. Bouabsa, C. Marignac, R. Chabbi, and M. Cuney, "The Filfila (NE Algeria) topaz-bearing granites and their rare metal minerals: Petrologic and metallogenic implications," *Journal of African Earth Sciences*, vol. 56, no. 2-3, pp. 107–113, 2010.

[71] Z.-Y. Zhu, R.-C. Wang, X.-D. Che, J.-C. Zhu, X.-L. Wei, and X. Huang, "Magmatic-hydrothermal rare-element mineralization in the Songshugang granite (northeastern Jiangxi, China): Insights from an electron-microprobe study of Nb-Ta-Zr minerals," *Ore Geology Reviews*, vol. 65, no. 4, pp. 749–760, 2015.

[72] C. Marignac, D. E. Aïssa, L. Bouabsa, M. Kesraoui, and S. Nedjari, "The Hoggar Gold and Rare Metals Metallogenic Province of the Pan-African Tuareg Shield (Central Sahara, South Algeria): An Early Cambrian Echo of the Late Ediacaran Murzukian Event?" in *Mineral Deposits of North Africa*, Mineral Resource Reviews, pp. 371–404, Springer International Publishing, Cham, Switzerland, 2016.

[73] D. Ohnenstetter and P. Piantone, "Pyrochlore-group minerals in the Beauvoir peraluminous leucogranite, Massif Central, France," *The Canadian Mineralogist*, vol. 30, no. 3, pp. 771–784, 1992.

[74] B. Charoy, M. Chaussidon, C. Le Carlier de Veslud, and J. L. Duthou, "Evidence of Sr mobility in and around the albite-lepidolite-topaz granite of Beauvoir (France): An in-situ ion and electron probe study of secondary Sr-rich phosphates," *Contributions to Mineralogy and Petrology*, vol. 145, no. 6, pp. 673–690, 2003.

[75] K. J. Jackson and H. C. Helgeson, "Chemical and thermodynamic constraints on the hydrothermal transport and deposition of tin: I. Calculation of the solubility of cassiterite at high pressures and temperatures," *Geochimica et Cosmochimica Acta*, vol. 49, no. 1, pp. 1–22, 1985.

[76] C. A. Heinrich, "The chemistry of hydrothermal tin(-tungsten) ore deposition," *Economic Geology*, vol. 85, no. 3, pp. 457–481, 1990.

[77] D. London, R. L. Hervig, and G. B. Morgan VI, "Melt-vapor solubilities and elemental partitioning in peraluminous granite-pegmatite systems: experimental results with Macusani glass at 200 MPa," *Contributions to Mineralogy and Petrology*, vol. 99, no. 3, pp. 360–373, 1988.

[78] V. I. Kovalenko, G. M. Tsareva, and M. Cuney, "Major-, trace elements and water in the magma of the Beauvoir rare metal granite, France (melt inclusion data)," *Doklady Akademii Nauk*, vol. 358, no. 5, pp. 667–671, 1998.

[79] G. P. Zaraisky, V. Korzhinskaya, and N. Kotova, "Experimental studies of Ta_2O_5 and columbite-tantalite solubility in fluoride solutions from 300 to 550°C and 50 to 100 MPa," *Mineralogy and Petrology*, vol. 99, no. 3-4, pp. 287–300, 2010.

[80] A. Timofeev, A. A. Migdisov, and A. E. Williams-Jones, "An experimental study of the solubility and speciation of niobium in fluoride-bearing aqueous solutions at elevated temperature," *Geochimica et Cosmochimica Acta*, vol. 158, pp. 103–111, 2015.